CHALMERS
UNIVERSITY OF TECHNOLOGY

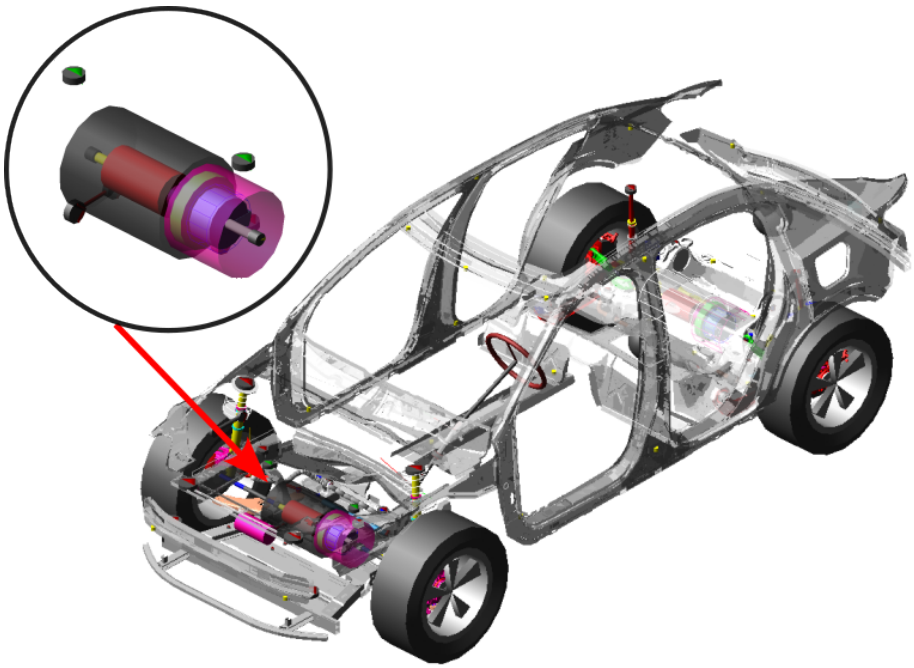

Investigating modal requirements for vibration isolation in driveline installations

A parametric study of the correlation between modal quantities and dynamic response

Master's thesis in Applied Mechanics

LINN BLOM
OSCAR HALLBERG

DEPARTMENT OF MECHANICS AND MARITIME SCIENCES
CHALMERS UNIVERSITY OF TECHNOLOGY
Gothenburg, Sweden 2023
www.chalmers.se

MASTER'S THESIS 2023

Investigating modal requirements for vibration isolation in driveline installations

A parametric study of the correlation between modal quantities and dynamic response

LINN BLOM
OSCAR HALLBERG

CHALMERS
UNIVERSITY OF TECHNOLOGY

Department of Mechanics and Maritime Sciences
Division of Dynamics
CHALMERS UNIVERSITY OF TECHNOLOGY
Gothenburg, Sweden 2023

Investigating modal requirements for vibration isolation in driveline installations
A parametric study of the correlation between modal quantities and dynamic response
LINN BLOM
OSCAR HALLBERG

Supervisor: Dr. Anders Hägglund, Volvo Cars Corporation
Co-supervisor: Markus Kvist, M.Sc. Volvo Cars Corporation
Examiner: Prof. Håkan Johansson, Division of Dynamics

Master's Thesis 2023
Department of Mechanics and Maritime Sciences
Division of Dynamics
Chalmers University of Technology
SE-412 96 Gothenburg
Telephone +46 31 772 1000

Cover: **A model of a car with the driveline installation highlighted.**

Typeset in LaTeX
Printed by Chalmers Reproservice
Gothenburg, Sweden 2023

Investigating modal requirements for vibration isolation in driveline installations
A parametric study of the correlation between modal quantities and dynamic response
LINN BLOM
OSCAR HALLBERG
Department of Mechanincs and Maritime Sciences
Chalmers University of Technology

Abstract

The *Performance and Driveability* team at Volvo Cars Corporations works to ensure a smooth and comfort ride for the vehicle occupants. This includes to isolate longitudinal vibrations that can be perceived as disturbing. This thesis focuses on finding a modal requirement on the engine set-up that can declare the time domain performance regarding vibration isolation. A parametric study has been conducted to see how deviations in parameter values affect the performance of the driveline configuration. This was done with the Latin Hypercube Sampling method to generate designs that was simulated in Adams View. From Adams, modal data and time domain data were obtained and the performance was evaluated by using the vibration dose value in the longitudinal direction, which is known to be a good measurement of comfort in vehicles.

Modal kinetic energy and participation factors are shown to be good measurements of the coupling between eigenmodes, and their different terms are tried as modal requirement. No definitive value was obtained but an idea is that a combination of different modal terms could perform well regarding correlation. The parametric study shows that inertia properties heavily influence the performance of the engine set-up and that a well performing set-up is less sensitive to variations than a worse performing one. In addition, this thesis work has provided a framework for modal analysis that can be used by Volvo Cars Corporations in further research within this subject or for other purposes.

Keywords: Vibration isolation, Driveline installation, Modal kinetic energy, Participation factor, Modal analysis, Adams View, Rigid body dynamics, Spearman's rank correlation.

Acknowledgements

This master's thesis was carried out in the spring of 2023 for the *Department of Mechanics and Maritime Sciences* at the University of Chalmers in Gothenburg. The work was done in collaboration with Volvo Cars Corporation and the majority of the work was conducted at their office in Torslanda, Sweden.

We would like to thank the whole *Performance & Driveability and Charging Performance* team for a successful spring filled with joy and laughter. Especially a big thanks to our supervisors Anders Hägglund and Markus Kvist for their tremendous willing to assist us in our work and for always being present whenever we needed their guidance. Last but not least we want to show our gratitude to our examiner Håkan Johansson who has been very supportive throughout the work and spent both days and nights to answer all of our questions.

Linn Blom, Gothenburg, June 2023
Oscar Hallberg, Gothenburg, June 2023

Nomenclature

Below is the nomenclature of acronyms and symbols that have been used throughout this thesis.

Acronyms

COG	Centre Of Gravity
DOE	Design Of Experiments
DOF	Degree Of Freedom
LHS	Latin Hypercube Sampling
RMQ	Root Mean Quad
RMS	Root Mean Square
VCC	Volvo Car Corporation
VDV	Vibration Dose Value

Symbols

θ	Rotational DOF around y-axis
ρ	Spearman's correlation number
Φ	Matrix with eigenmodes
φ	Rotational DOF around z-axis
ψ	Rotational DOF around x-axis
ω	Eigenfrequency
$\mathbf{A}$	Rotation matrix
$\mathbf{C}$	Damping matrix
E_{ij}	Modal kinetic energy in DOF i for mode j
$\mathbf{F}$	Force vector
$\mathbf{I}$	Inertia matrix

I_{ij}	Inertia terms with $i, j = x, y, z$
$\mathbf{K}$	Stiffness matrix
k	Local stiffness in spring element
$\mathbf{M}$	Mass matrix
M	Moments from spring forces
m	Local mass of body
p_{ij}	Participation factor in DOF i for mode j
$\mathbf{q}$	State vector
$\mathbf{R}$	Distance from COG to spring attachment
R_x	Rotation around x-axis
R_y	Rotation around y-axis
R_z	Rotation around z-axis
r_i	Dimension of body in directions $i = 1, 2, 3$
$\mathbf{T}$	Torque vector
t	Time
U	Potential energy

Contents

List of Figures

List of Tables

1
Introduction

In this chapter, the background to the work will be introduced together with the problem formulation and purpose of the thesis. Additionally, some limitations will be presented.

1.1 Background

Starting in 2035, a significant measure has been implemented, preventing new cars and vans from emitting any CO2 during use, as a result of the European Parliament's support for the European Commission's zero-emissions vision, which was announced in June 2022 [1]. This was made in order to be able to reach the goal of the transport sector; to be climate neutral by 2050. Because of this, companies in the automotive industry now have to start replacing the combustion engines with electrical engines. For Volvo Cars Corporation (VCC), the electrification has already started, and the ambition is to be a fully electric car company already by 2030, which means a lot of new challenges [2].

The strategic direction of VCC is *"Freedom to move in a Personal, Sustainable and Safe way"*. Personal includes the users' final experiences of the cars, such as the comfort and noise when driving, as well as the vehicle dynamics. One of the challenges is to continue to enable a smooth and comfortable ride for the passengers. This is one of many things that the *Performance & Drivability and Charging Performance* team, which is a part of the Personal Centre within Research & Development at VCC, is responsible for. One way of doing this is to try to verify and predict the longitudinal vehicle characteristics. This includes the dynamical behaviour of the engine and how to predict the transients affecting the occupants when the engine starts to move. Movement of the engine often occurs when e.g. driving on an uneven road or a sudden speed increase, and to obtain a smooth ride, resonance should be avoided.

Today, problems regarding vibration isolation for the driveline installation are often solved in an early phase of the process and often by doing easy observations of modal alignments, i.e. a systems modal energies in different directions. By providing VCC with requirements regarding relations between a modal quantity and the time domain performance, the work could be simplified. Hopefully, the requirements can be formulated in a probabilistic sense that provides a certain level of vibration isolation distribution.

Previously, different work with similar purpose has already been done. In 2020, Federico Longoni wrote his master's thesis *Powertrain Modal Analysis for the Definition of the Requirements in the Vehicle Driveability Study* and in 2022 his work was published in

a condensed format [3]. Longoni focused on finding a modal requirement by using analytical solutions and investigating the benefits of fully decoupled systems. This includes inventing new modal properties that can declare the time domain performance. Now Longoni's work will be continued with numerical solutions as well as a parametric study of the correlation between modal quantities and dynamic response.

1.2 Purpose

The main purpose of this thesis is to help VCC to provide a smoother ride for the vehicle occupants. A smooth and comfort ride are important aspects in the overall impression of the vehicle, and therefore VCC puts a lot of effort in reducing vibrations that can be perceived as disturbing for the occupants. This thesis focuses on the early stage of the design process and will create a fundament for further work within this research field.

The aim is to find a measurable quantity in the modal domain that can predict the time domain performance regarding vibration isolation in certain directions for different excitation modes. This allows developers to get an understanding of the dynamic behaviour without running expensive and time-consuming simulations. When investigating the modal characteristics, coupling phenomena will be considered to see how well different mode shapes correlate. Additionally, design configurations containing double modes (two modes with similar eigenfrequencies) will be investigated to see how such set-ups tell anything about the dynamic performance.

Another aim is to carry out a sensitivity analysis to see how different design parameters affect the dynamic performance of the vehicle. The value of a design parameter can vary due to e.g. temperature, moist and dust. The intention is to see how these deviations and uncertainties in parameter values may affect the behaviour regarding vibration isolation. Another design change can be if a mass is added to the set-up. The goal is then to easily be able to determine whether such modifications will affect the outcome poorly or not.

To obtain the aim and fulfil the purpose, a numerical model that captures the dynamic phenomena of a vehicle driveline installation will be provided. The findings from the model can then be used in further research and development, enabling a smoother ride for the vehicle occupants. To this end, the model will be implemented in a general-purpose dynamics simulation software, to be used for other purposes as well, not only the ones covered in the scope of this thesis.

1.3 Research questions

Taking the purpose into account, the main research questions for this thesis can be established as follows:

1. What can be a suitable quantity in the modal domain to predict the time domain performance regarding vibration isolation for a driveline installation?

2. How do deviations in parameter values affect the dynamic response of an engine set-up?

1.4 Limitations

Like every numerical model, the amount of complexity taken into account is a factor that will affect the reliability of the final results. During this thesis, the complexity used in the model will successively increase depending on how challenging and time consuming the early stages of the project turned out to be. This means that no specific goal on the amount of complexity will be decided in advance.

There are some delimitations that will be considered throughout the entire project. This is for example that damping will not be considered in the models and simulations. Additionally, a linear approximation of the system is implemented despite non-linear behaviour may exist. Also, only rigid bodies will be used. Further on, the scope of this project does not cover an analysis of the complete driveline installation. Instead, simple models will be generated to give an understanding of the fundamental dynamic behaviour of a general system. This means that the driveline installation will be approximated as a single rigid body that captures the most fundamental behaviour of an engine set-up. Parameter values will be chosen strategically to get close to a standard configuration.

2

Theory

This chapter describes theory about vehicle dynamics and properties used to calculate modal quantities. Also, parameters for statistical analysis will be explained.

2.1 Vehicle dynamics

Vehicle dynamics is an engineering field that deals with motions of vehicles during different driving conditions [4]. The field contains models and quantities that are designed to explain vehicle phenomena from a mechanical point of view. This chapter covers the most important vehicle dynamics concepts used in this thesis.

2.1.1 Coordinate system

The coordinate system of a vehicle is usually defined by VCC as depicted in figure 2.1. This means an x-direction pointing backwards, y-direction pointing to the right and z-direction pointing upwards. Often in vehicle industries, the axes are called *roll*, *pitch* and *yaw*, respectively. Note that the coordinate system in figure 2.1 shows a local system for the powertrain. The global coordinate system is usually positioned a distance in front of the car.

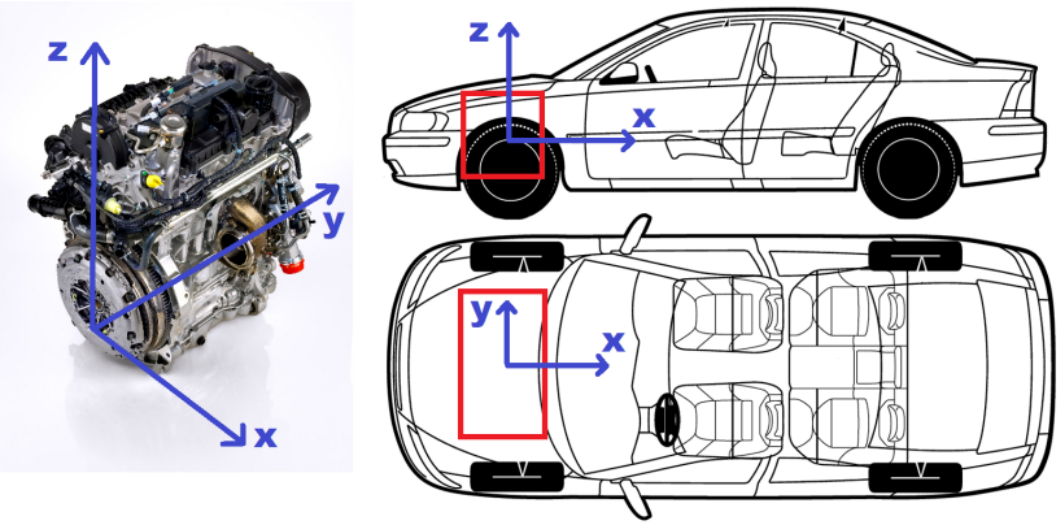

Figure 2.1: Coordinate system of a car. The red square represents the position of the powertrain [3].

Translating this coordinate system into physical terms, some typical load cases can be identified. This thesis mainly focuses on torque around the y-axis and force in z-direction. The practical representation of this can be a sudden speed increase or driving over a bump in the road.

2.1.2 Engine mounts

There are different types of engine mounts used in the vehicle industry. One way to represent them is by using bushing elements. A bushing can be considered as an anisotropic concentrated spring with different stiffnesses in all different degrees of freedom, DOFs. This means that the local stiffness matrix for a bushing can be expressed as

$$\mathbf{K} = \begin{bmatrix} k_{xx} & 0 & 0 & 0 & 0 & 0 \\ 0 & k_{yy} & 0 & 0 & 0 & 0 \\ 0 & 0 & k_{zz} & 0 & 0 & 0 \\ 0 & 0 & 0 & k_{\psi\psi} & 0 & 0 \\ 0 & 0 & 0 & 0 & k_{\theta\theta} & 0 \\ 0 & 0 & 0 & 0 & 0 & k_{\varphi\varphi} \end{bmatrix} \tag{2.1}$$

In many vehicles, a typical engine set-up consists of 3-5 bushing elements placed strategically to ensure a good performance. The location of the bushings as well as the orientation of the principal axes will contribute to a stiffness matrix in global coordinates with off-diagonal terms as well. To obtain a full stiffness matrix for the model, all local stiffness matrices are added together. This is permitted according to the law of superposition.

The bushing elements can look different. One type is like a cushion that the engine rests on which restricts the motion in that point. Other shapes can be rigid rods connected between the driveline installation and the chassis of the car. These are usually stiff in one end making it possible to assume the bar as one bushing element as well. All bushing elements are usually made of rubber or elastomers which provides a degree of damping, but that is neglected in this thesis work.

2.2 Modal analysis

Modal analysis is a commonly used process for determining dynamical attributes in the frequency domain of a system. This includes eigenfrequencies, eigenmodes and damping factors, which are also known as the system's modal data [5]. The modal data is used to determine the dynamical behaviour of a body.

2.2.1 Modal coordinates

To determine the properties of a general system, the equation of motion for free vibration is used

$$\mathbf{M}\ddot{\mathbf{q}} + \mathbf{C}\dot{\mathbf{q}} + \mathbf{K}\mathbf{q} = \mathbf{0} \tag{2.2}$$

where $\mathbf{M}$, $\mathbf{C}$ and $\mathbf{K}$ are the mass, damping and stiffness matrices, respectively. The vector $\mathbf{q}$ is the state vector containing all DOFs for the system. In this thesis work, damping will

be neglected meaning that $\mathbf{C} = \mathbf{0}$. If harmonic motion is assumed, an ansatz for the state vector $\mathbf{q}$ can be made as

$$\mathbf{q} = \Phi \cos(\omega t) \tag{2.3}$$

Performing the derivatives in equation (2.2) and letting the system be undamped, the following eigenvalue problem can be formulated as

$$(\mathbf{K} - \omega^2 \mathbf{M})\Phi = \mathbf{0} \tag{2.4}$$

where ω denotes the natural frequency and Φ denotes the corresponding eigenmode or mode shape. For a rigid body system, the number of eigenvalues corresponds to the number of DOFs [6]. To avoid getting a trivial solution $\Phi = \mathbf{0}$, the eigenvalues are calculated as the algebraic equation below.

$$\det(\mathbf{K} - \omega^2 \mathbf{M}) = 0 \tag{2.5}$$

This gives the eigenfrequency ω_i for the i:th mode which makes it possible to calculate the mode shape Φ_i. Note that the eigenmode is not a unique solution. It can be multiplied with a constant multiplier and still solve equation (2.4). For convenience, the mode shape is normalized.

For the time domain solution, a combination of the different mode shapes is used. From equation (2.3), it can be extracted that the motion in DOF k for an N-DOF system is a combination of every mode shape in line with the following equation [6]

$$q_k(t) = \sum_{i=1}^{N} \Phi_i^{(k)} \cos(\omega_i t) \tag{2.6}$$

where $\Phi_i^{(k)}$ means DOF k of mode i. In the equation above, every mode shape with its natural frequency contributes to a movement for every DOF. This indicates that the coupling of modes and their impurity in a specific direction may be interesting to evaluate the dynamic performance. Two quantities that use the eigenmodes to describe a systems behaviour are *Participation factors* and *Modal kinetic energy*, which will be further explained in the following sections.

2.2.2 Participation factors

Participation factors are nondimensional scalars that can be used as a measurement to describe the contribution of a specific mode to a specific state [7]. With other words, it is a factor that expresses the amount of movement in a specific direction for a specific mode. One way of using it is to describe the coupling between a system's eigenmodes. The expression for the participation factor in mode k and state i is defined as

$$p_{ki} := \phi_{ik}^L \phi_{ki}^R \tag{2.7}$$

where ϕ_{ik}^L is the left eigenmode and ϕ_{ki}^R is the right one. The term ϕ_{ki}^R corresponds to $\Phi_i^{(k)}$ in equation (2.6) but it is written with index notation for convenience. The definition of the left and right eigenmode is

$$[\Phi^L][\Phi^R] = [\mathbf{I}] \tag{2.8}$$

where $\mathbf{I}$ is the identity matrix. This means that Φ^R can be considered as the regular eigenmode matrix that is solved for in equation (2.4) and Φ^L its inverse. Participation factors can be expressed as an $N \times N$-matrix where N is the number of DOFs in the system. The highest value in each column indicates the most dominant direction for that specific mode. The columns add up to 1 which means that each number represents how many percentages of the movement that is in that certain direction. An example of a participation factor matrix can be seen in table 2.1 where the values are stated in percentage.

Table 2.1: An example of a participation factor matrix with the most dominant directions in each mode marked in green [3].

	Rx-mode	Y-mode	Ry-mode	Rz-mode	X-mode	Z-mode
X-DOF	0.46	2.72	0.47	9.93	**67.47**	18.95
Y-DOF	1.11	**92.94**	0.39	0.26	5.18	0.12
Z-DOF	0.01	0.75	20.27	0.00	14.01	**64.96**
Rx-DOF	**94.91**	1.45	0.67	2.74	0.00	0.23
Ry-DOF	0.64	1.07	**77.79**	1.44	4.30	14.76
Rz-DOF	2.87	1.07	0.41	**85.63**	9.04	0.98
Eigenvalue [Hz]	5.78	9.32	12.27	19.12	22.86	26.50

2.2.3 Modal kinetic energy

Another measurement that can be used to describe the motion of the system is *Modal kinetic energy*. The kinetic energy in a system is distributed into the different modes. The system's kinetic energy can be written as

$$\Gamma_i = \frac{1}{2}\dot{\mathbf{q}}^T \mathbf{M}\dot{\mathbf{q}} \tag{2.9}$$

Taking the derivative of the state vector in equation (2.6), the kinetic energy can be stated as

$$T = \frac{1}{2}\left(\sum_i^N \omega_i \Phi_i \sin(\omega_i t)\right)^T \mathbf{M}\left(\sum_i^N \omega_i \Phi_i \sin(\omega_i t)\right) \tag{2.10}$$

which can be viewed as a sum of contributions from different modes

$$T = \sum_i \Gamma_i \sin^2(\omega_i t) \qquad \text{with} \qquad \Gamma_i = \frac{\omega_i^2}{2}\Phi_i^T \mathbf{M}\Phi_i \tag{2.11}$$

where Γ_i is the kinetic energy of mode i, ω_i is the eigenfrequency, Φ_i is the mode shape vector of mode i and $\mathbf{M}$ is the mass matrix of the system. The expression explaining how the percentage of kinetic energy contribution for a part to mode i is defined in Adams View and can be found in the equation below [8].

$$E_i^k = 100\Big(\frac{\omega_i^2 \cdot \kappa_k}{\Gamma_i}\Big) \tag{2.12}$$

Here k is the direction, i.e. the amount of kinetic energy in a specific DOF for that mode. The term κ_k is the contribution from a specific DOF and is calculated as following for the translating DOFs x, y and z.

$$\kappa_k = \frac{1}{2}\big[m\Phi_i^{(k)}\Phi_i^{(k)}\big] \qquad \text{for } k = x,y,z \tag{2.13}$$

For the rotational DOFs, Rx, Ry and Rz, the moment of inertia is used instead of the mass, which means that κ is expressed as

$$\kappa_{kl} = \frac{1}{2}\big[\Phi_i^{(k)} I_{ef} \Phi_i^{(l)}\big] \qquad \text{for } e,f = x,y,z \tag{2.14}$$

where k is the DOF for rotation around the e-axis and l is the DOF for rotation around the f-axis. For a three-dimensional model, the kinetic energy contribution is divided into nine κ_k components in total, one for every DOF as well as three mixed rotational terms. The mixed terms arise when $k \neq l$ in equation (2.14). Since the sum of all contributions of kinetic energy from each DOF is equal to 100% in a specific mode shape, modal kinetic energy is a great measure to use when trying to understand why the system exhibit the specific movement patterns that it does. It becomes a straightforward approach for explaining the relative importance of every specific DOF.

2.2.4 Difference: *Modal kinetic energy* and *Participation factors*

At first glance, participation factors and modal kinetic energy seems to tell the same thing about a model, but there are some major differences. The most significant difference is that the modal kinetic energy matrix contains the mixed rotational terms K_{Rxy}, K_{Rxz} and K_{Ryz} [8]. However, these terms have no obvious physical meaning, and can be both positive and negative. A negative energy is unphysical, but it helps to make the columns and rows to sum up to 100% [3]. These terms exist in a 6-DOF model, but in a 3-DOF model they vanish. This means that in a 3-DOF case, the modal kinetic energy and the participation factors are the same, while there is a difference in the 6-DOF case.

2.3 Rotation matrices and Euler angles

General rotation of e.g. bushings, springs or rigid bodies can be described with Euler angles. The idea is that a body rotates around a body-fixed coordinate system in a specific consecutive order. In this thesis, the rotation 3-1-3 is used. This means that the body rotates around the z-axis of a body-fixed xyz frame that coincide with the global XYZ frame. This creates a new body-fixed frame denoted $x'y'z'$. The body then rotates around the x'-axis leading to the $x''y''z''$ frame. Finally, the body rotates around the z''-axis to generate a new xyz frame posterior to rotation. The reason why this rotation scheme is used is because Adams View wants that as input. Other commonly used rotation schemes are 3-2-3 and 3-2-1, the latter one called *roll-pitch-yaw* [9].

A rotation matrix can be computed for rotation around the different axes. Using the global coordinate axes for rotation, the matrices can be computed as follows

$$\mathbf{A}_x(\psi) = \begin{bmatrix} 1 & 0 & 0 \\ 0 & \cos(\psi) & \sin(\psi) \\ 0 & -\sin(\psi) & \cos(\psi) \end{bmatrix}, \qquad \mathbf{A}_y(\theta) = \begin{bmatrix} \cos(\theta) & 0 & -\sin(\theta) \\ 0 & 1 & 0 \\ \sin(\theta) & 0 & \cos(\theta)) \end{bmatrix}$$

$$\mathbf{A}_z(\varphi) = \begin{bmatrix} \cos(\varphi) & \sin(\varphi) & 0 \\ -\sin(\varphi) & \cos(\varphi) & 0 \\ 0 & 0 & 1 \end{bmatrix}$$

When computing a full rotation matrix, the included rotations are multiplied with each other. Note that rotations with Euler angles is not a commutative operation, meaning that the order of the matrices matters. Subsequent matrices are multiplied from the left. This means that a 3-1-3 rotation scheme for the angles α, β and γ is calculated as

$$\mathbf{A}(\alpha,\beta,\gamma) = \mathbf{A}_z(\gamma)\,\mathbf{A}_x(\beta)\,\mathbf{A}_z(\alpha) \tag{2.15}$$

One issue with the 3-1-3 rotation scheme is that singularities easily can arise. This happens when the second rotation, the one around the x-axis, makes the first and third axes coincide with each other. One example of this is when the second rotation is 0 degrees. When this happens, the two other rotations cannot be separated.

A useful property of rotation matrices is that they are orthogonal, meaning that the inverse is equal to the transpose of the matrix. This means that the coordinate change can go back and forth by using the rotation matrix in equation (2.15). This gives the relation

$$\begin{pmatrix} e_x \\ e_y \\ e_z \end{pmatrix} = \mathbf{A}(\alpha,\beta,\gamma) \begin{pmatrix} e_X \\ e_Y \\ e_Z \end{pmatrix} \qquad \Rightarrow \qquad \begin{pmatrix} e_X \\ e_Y \\ e_Z \end{pmatrix} = \mathbf{A}^T(\alpha,\beta,\gamma) \begin{pmatrix} e_x \\ e_y \\ e_z \end{pmatrix} \tag{2.16}$$

2.4 Vibration dose value

One commonly used measurement when performing vibration analyses is *Vibration dose value* (VDV), which is used to catch the behaviour of a decided parameter over time. In this case force in x-direction is considered, since it is the movement and vibration in the longitudinal direction that is the most interesting quantity regarding driving experience [10]. In that case, the unit of the VDV becomes $[\mathrm{kg\,m\,s^{-7/4}}]$ and the formula is defined as follows

$$\mathrm{VDV} = \sqrt[4]{\int_0^T F_x^4(t)dt} \tag{2.17}$$

VDVD is more sensitive to peak values compared to an RMS-value [11]. This makes it a good and common measurement in the vehicle industry for vibration injuries and comfort [12]. It is commonly measured on the seat surface close to the end of the spine in both longitudinal, lateral and vertical direction in line with ISO 2631-1. Measurements are also made on the seat floor close to where the feet usually are positioned. In conclusion,

using VDV is a good and common method for measuring the experienced comfort during a ride and that is why it will be used frequently in this thesis report.

2.5 Latin hypercube sampling

Latin hypercube sampling (LHS) is a limited version of the Monte Carlo method. It is described as an almost randomized statistical sampling method, sometimes called a stratified sampling. Figure 2.2 shows LHS compared to a Monte Carlo simulation. This indicates that Monte Carlo is an uncontrolled randomized sampling while LHS provides a more even distribution [13]. The figure shows the distribution of 15 points from five different boxes chosen with both methods.

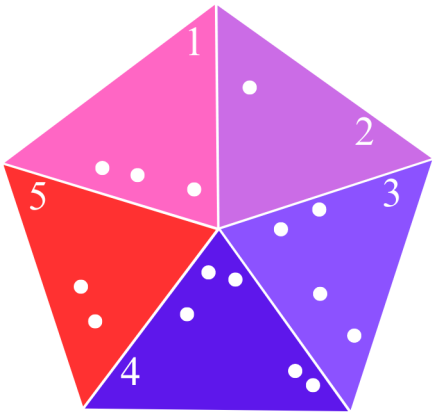

(a) Example of a Monte Carlo sampling.

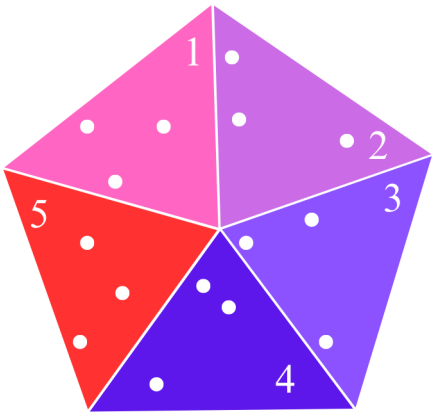

(b) Example of a Latin Hypercube sampling.

Figure 2.2: Example of how the difference between a random sampling and a stratified sampling can look like [13]. In this sampling 15 points should be chosen from five different boxes.

By defining the number of parameters, wanted designs and ranges for each parameter, the LHS tries to distribute the designs in a way such that most of the different possible combinations are covered [14]. All parameters are divided uniformly and then randomly combined with each other, where each level of a parameter is used only once. An example of an LHS with two independent parameters is visualized in figure 2.3. This clearly shows that the data points are evenly, but still randomly, distributed in the domain with the LHS method.

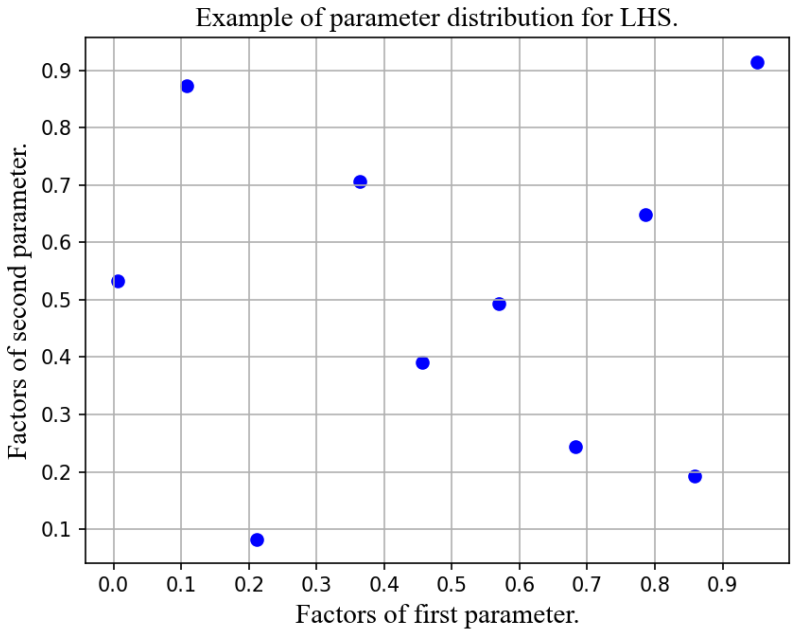

Figure 2.3: An example of a LHS with two factors and ten sample points.

One of the greatest advantages of using LHS when doing a design of experiment (DOE) is that the user freely can choose the number of wanted designs. This means that the computational time will be much shorter than for example for a full factorial sampling method where all possible combinations are under consideration [15].

2.6 Spearman's rank correlation

The Spearman's rank correlation coefficient is a measurement of the correlation between two discrete data sets. In contrast to other common correlation methods, rank correlation does not apply any curve fitting. Instead, only the monotonicity is studied which means that a high value (close to 1) implies that an increase in data set x also implies an increase in data set y. The correlation coefficient can be calculated as follows [16]

$$\rho = 1 - \frac{6\sum D_i^2}{n(n^2-1)} \tag{2.18}$$

The formula is based on the rank of the data set, which means that every value is transformed to an individual integer between 1 and n in size order where n is the number of points in the data set. This is called an ordinal scale which collects every data point in size order without any concerns about the interval between them. The variable D_i in equation (2.18) represents the difference between the rank of the x-value and the rank of the y-value for the i:th data point. The correlation coefficient takes a value of $\rho \in [-1,1]$ where both 1 and -1 represents a good correlation. The difference between them is whether data set y constantly *increases* or *decreases* when data set x increases. A correlation coefficient of 0 means no correlation at all.

3
Methods

In this chapter, the methods that were used during the work will be described. This includes both analytical calculations and how numerical models were created and combined with a framework in Python to receive the results.

3.1 Methodology - overview

The dynamic behaviour of an engine set-up can be obtained with numerical models subjected to a loading scenario. To evaluate the performance regarding vibration isolation in the longitudinal direction, a wide range of set-ups have been tested to see how variations in parameter values affect the dynamic behaviour. The complete dynamic response was evaluated but it is the longitudinal characteristics that mainly have been under consideration. The prime goal with the methodology have been to be able to produce the models and evaluate a wide range of set-ups in a systematic way.

At first, a two-dimensional model with three DOFs was under consideration. The idea was to investigate the 3-DOF model to get an understanding of the basic fundaments of the dynamic behaviour. It was also beneficial to begin with implementing the framework for a model in two dimensions since the results from that simulation are easier to verify and validate against reality compared to a more complex model. Therefore, all steps were carried out in two dimensions before continuing with a 6-DOF model in three dimensions. In conclusion, the 3-DOF model was used to verify the reliance of the framework while the 6-DOF model was used to replicate a real driveline installation and draw conclusions on the results.

To obtain results, two different tools have been essential for the work. The programming language Python have been used for pre-processing, post-processing and parameter variations. Analytical calculations have also been carried out to verify the numerical results. All simulations have been made with the multibody dynamics simulation tool Adams View. This tool can generate both modal information as well as time history data after a loading event.

3.1.1 Framework for model simulation

To be able to run a wide range of different set-ups, a framework for model simulations have been conducted. The intention is that this framework can be used by VCC in further development with other intended outcomes than the ones in this thesis work. A schematic

picture of the framework can be seen in figure 3.1. Note that each box contains a bunch of happenings and that this only shows the fundamental structure of the workflow. The schematic picture can be seen as an overview of the work and each detail will be further explained later.

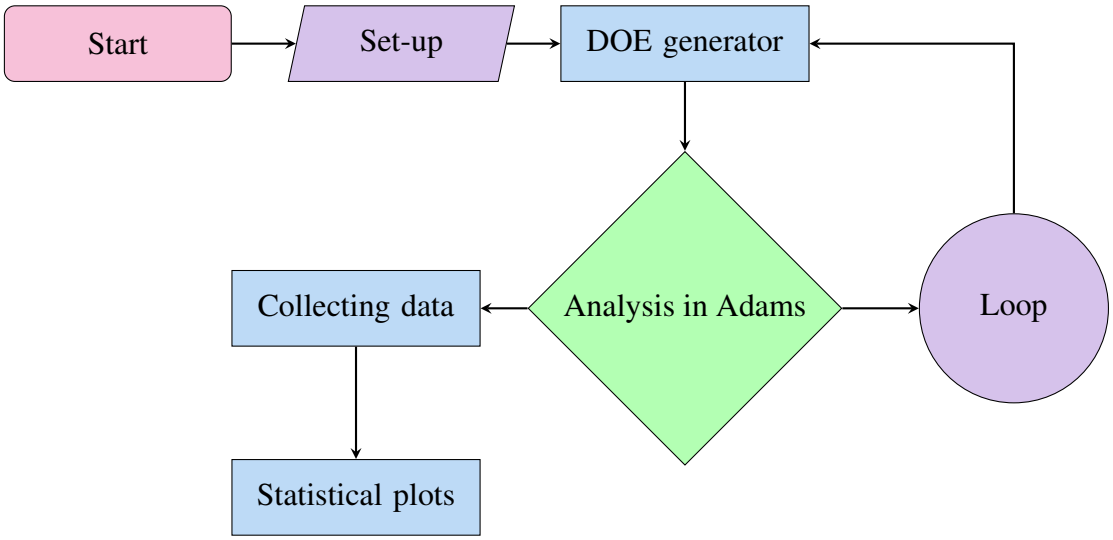

Figure 3.1: Workflow showing how the model simulations are done, from inserting the wanted set up to collecting the wanted data and creating statistical plots.

First step when wanting to start the simulation is to decide a set-up of the model in a Python script. This includes geometrical properties, parameters for stiffness elements, loading scenario as well as the number of wanted samples. The design parameters are stated with upper and lower bounds to be able to generate a DOE. Before starting the DOE generator, a global stiffness matrix is calculated from the contribution of all local stiffness matrices for the stiffness elements. This is done to satisfy the input syntax in Adams View. Every design configuration is then simulated in Adams View and after each run, all requested data is assembled, including both time- and modal quantities. The data is postprocessed to obtain manageable information. This includes e.g. reordering the modes and calculate participation factors. When the DOE is finished and all the wanted data is collected, it is possible to do further statistical investigations, including correlation plots.

The modeller has some freedom regarding the input to the python code. To perform the LHS-sampling, a lower and upper bound on every design parameter is chosen by the modeller as well as number of samples. These bounds decide how much the value of each design parameter is allowed to vary during the DOE and how many different set-ups that should be included. The loading applied to the model can be chosen as a pure torque impulse, a force with specified duration time in addition with an attacking position, or a combination of both. All together the applied impulse will be re-calculated into initial conditions in each direction.

3.2 3-DOF model

To begin with, a 3-DOF system, consisting of a two-dimensional rigid body subjected to three springs, according to figure 3.2, was investigated. The three DOFs consist of translation in x- and z-direction as well as rotation around the y-axis. The positions of all three springs are arbitrary along the edge of the body, and one of the springs is rotated with the angle γ. This enables the opportunity to find as general results as possible. In addition, it is also possible to change the dimensions of the rigid body. The global coordinate system is located in the centre of mass and the three blue systems in figure 3.2 are local coordinate systems, one for each spring. The coordinate systems in the springs are body fixed and move with the springs.

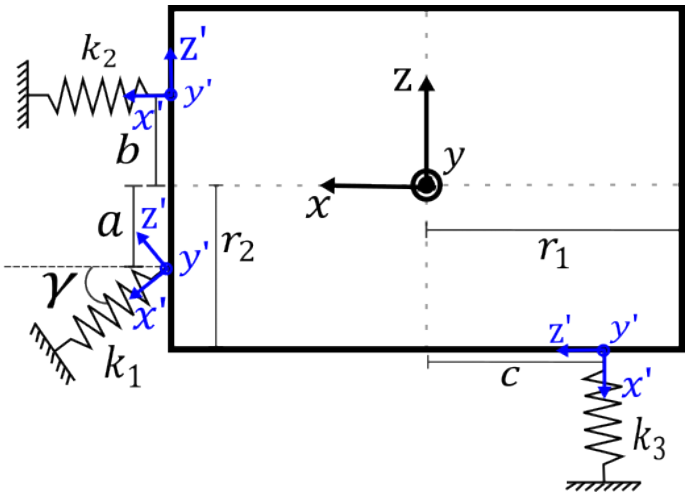

Figure 3.2: The studied 3-DOF system consisting of three springs subjected to a rigid body.

3.2.1 Analytical expressions of mass- and stiffness matrices

To gain an understanding of the behaviour of the two-dimensional system, analytical expressions of the stiffness- and mass matrices were conducted. The goal is to describe the system in a linear form as

$$\mathbf{M}\ddot{\mathbf{q}} + \mathbf{K}\mathbf{q} = \mathbf{0} \tag{3.1}$$

where $\mathbf{M}$ is the mass matrix, $\mathbf{K}$ is the stiffness matrix and $\mathbf{q}$ is the state vector defined for the 3-DOF system as

$$\mathbf{q} = [x, \quad z, \quad \theta]^T \tag{3.2}$$

where θ is the rotation around the y-axis. Starting with the mass matrix $\mathbf{M}$, the system is considered to have the centre of mass in the middle of the geometry. This means that for the translational DOFs, the mass contribution is m, and for the rotational DOF the contribution is the moment of inertia I defined for a rectangle as

$$I = \frac{m\left(r_1^2 + r_2^2\right)}{3} \tag{3.3}$$

The mass matrix then becomes

$$\mathbf{M} = \begin{bmatrix} m & 0 & 0 \\ 0 & m & 0 \\ 0 & 0 & I \end{bmatrix} \tag{3.4}$$

Next step was to set up expressions for the position vectors to the attachment points of the springs, which can be described as following, according to the notations in figure 3.2

$$\mathbf{R_1} = \begin{bmatrix} r_1, & 0, & -a \end{bmatrix} \tag{3.5a}$$
$$\mathbf{R_2} = \begin{bmatrix} r_1, & 0, & b \end{bmatrix} \tag{3.5b}$$
$$\mathbf{R_3} = \begin{bmatrix} -c, & 0, & -r_2 \end{bmatrix} \tag{3.5c}$$

To establish the global stiffness matrix $\mathbf{K}$, the spring forces and torques from the springs were calculated. For each spring, a local coordinate system was introduced in the end of the springs that are attached to the rigid body, with the x-axis in the same direction as the spring, represented by the blue coordinate systems in figure 3.2. This resulted in the local stiffness matrix for each spring becoming

$$\mathbf{K}_{local} = \begin{bmatrix} k_i & 0 & 0 \\ 0 & 0 & 0 \\ 0 & 0 & 0 \end{bmatrix} \tag{3.6}$$

where $i = 1, 2, 3$ according to the stiffnesses in figure 3.2. To be able to determine the global stiffness matrix, the local ones needed to be translated into global coordinates, which could be done by using the following rotation matrix

$$\mathbf{A} = \begin{bmatrix} \cos\alpha & 0 & -\sin\alpha \\ 0 & 1 & 0 \\ \sin\alpha & 0 & \cos\alpha \end{bmatrix} \tag{3.7}$$

where α is the angle between the local and the global x-axis for each spring. By using the rotation matrix and the local stiffness matrix for a spring, the contribution to the global stiffness matrix for a specific spring could be calculated by using following equation

$$\mathbf{K}^i_{global} = \mathbf{A}^T \mathbf{K}^i_{local} \mathbf{A}\,, \qquad \text{for } i = 1, 2, 3 \tag{3.8}$$

After determine $\mathbf{K}^i_{global}$, the spring forces could be calculated in global coordinates according to

$$\mathbf{F}_i = \mathbf{K}^i_{global} \begin{bmatrix} x + \theta R_i(1) \\ 0 \\ z - \theta R_i(3) \end{bmatrix} \tag{3.9}$$

where R_i are the position vectors in equation (3.5). The vector in the equation above represents the elongation of the spring in different directions, considering both translational and rotational movement. After the expressions for the spring forces were calculated, the torques could be computed. The contribution from spring i can be determined with the cross product between the position vector and force vector according to

$$M_{yi} = \mathbf{R_i} \times \mathbf{F_i} \tag{3.10}$$

Taking the expressions for F_i and M_{yi}, the stiffness matrix can be computed. The composition is made by taking the x-components of every force and torque generated by the springs into the first row of the stiffness matrix. The state variable that each term is multiplied with determines the column. Doing this for each vector component, the final stiffness matrix becomes the one in equation (3.11). Note that the rows are ordered as 1, 3 and 5 to follow the convention for a 6-DOF model that will be analysed further on.

$$\mathbf{K} = \begin{bmatrix} K_{11} & K_{13} & K_{15} \\ K_{31} & K_{33} & K_{35} \\ K_{51} & K_{53} & K_{55} \end{bmatrix} \tag{3.11}$$

where

$$\begin{aligned}
K_{11} &= k_1 \cos^2\gamma + k_2 \\
K_{33} &= k_3 + k_1 \sin^2\gamma \\
K_{55} &= k_1(a\cos\gamma - r_1\sin\gamma)^2 + k_2 b^2 + k_3 c^2 \\
K_{13} &= K_{31} = k_1 \cos\gamma \sin\gamma \\
K_{15} &= K_{51} = k_1(r_1\cos\gamma\sin\gamma - a\cos^2\gamma) + k_2 b \\
K_{35} &= K_{53} = k_1(a\cos\gamma\sin\gamma - r_1\sin^2\gamma) + k_3 c
\end{aligned}$$

These equations are valid for all springs, the only difference is tha value of γ. For each spring, γ is the angle between the local x-axis, for that specific spring, and the global x-axis.

When the mass-matrix $\mathbf{M}$ and the stiffness matrix $\mathbf{K}$ are obtained, the eigenfrequencies and the eigenmodes can be calculated. This is done by solving the eigenvalue problem (2.4). The analytical modal quantities will be used as validation values towards the numerical model that will be implemented in Adams View.

3.2.2 Stiffness matrix from potential energy

The stiffness matrix can be obtained in different ways. The previous chapter introduced a stiffness matrix obtained from forces and moments generated from the springs. Now another method is explained that uses the potential energy. The relation from equation (3.12) is used to calculate the stiffness matrix [17]. The reason why two different methods are carried out is to compare results and verify if the models are correctly implemented.

$$\mathbf{K} = \sum_{i=1}^{n} \frac{\partial^2 U_i}{\partial \mathbf{q} \partial \mathbf{q}^T}\bigg|_{\mathbf{q}=\mathbf{0}} \tag{3.12}$$

In this equation, n is the number of springs, $\mathbf{q}$ is the state vector and U_i is the potential energy for a specific spring i, which is described as

$$U_i = \frac{1}{2} k_i (L - L_0)^2 \tag{3.13}$$

where L_0 is the original length of the spring. To express the actual length L of the spring, a vector between the two end points of the spring needs to be obtained. In figure 3.3, the notation used to express this is visualized for an arbitrary spring.

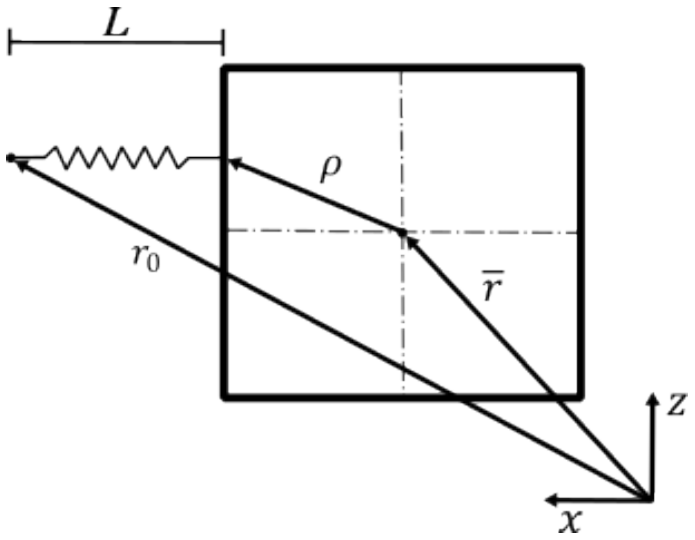

Figure 3.3: A one-spring system with notations needed to calculate the stiffness matrix.

The vector $\bar{\mathbf{r}}$ is the actual position of the body (simply $[x,z]$ for this 3-DOF system) and $\mathbf{r_0}$ is the position of the endpoint connected to the surrounding in global coordinates. The vector ρ is also in global coordinates and can be calculated as a rotation matrix times a vector with the spring position in body fixed coordinates as

$$\rho = \mathbf{A}\bar{\mathbf{u}} \tag{3.14}$$

where

$$\mathbf{A}(\theta) = \begin{bmatrix} \cos(\theta) & \sin(\theta) \\ -\sin(\theta) & \cos(\theta) \end{bmatrix}, \qquad \bar{\mathbf{u}} = [\bar{u}_x, \quad \bar{u}_z]^T \tag{3.15}$$

This means that the actual length of the linear spring can be expressed in global coordinates as

$$\mathbf{L} = \bar{\mathbf{r}} + \mathbf{A}\bar{\mathbf{u}} - \mathbf{r_0}, \qquad \text{with } L = |\mathbf{L}| \tag{3.16}$$

The derivatives of the potential energy U_i can then be computed as

$$\frac{\partial U_i}{\partial \mathbf{q}} = \frac{\partial U_i}{\partial L}\frac{\partial L}{\partial \mathbf{q}} = k_i(L - L_0)\frac{\partial L}{\partial \mathbf{q}} \tag{3.17}$$

$$\frac{\partial^2 U_i}{\partial \mathbf{q}\partial \mathbf{q}^T} = \{\text{Product rule}\} = k_i\frac{\partial L}{\partial \mathbf{q}}\frac{\partial L}{\partial \mathbf{q}^T} + k_i(L - L_0)\frac{\partial^2 L}{\partial \mathbf{q}\partial \mathbf{q}^T} \tag{3.18}$$

The derivative of the length L is computed for every degree of freedom which concludes that the final stiffness matrix can be expressed in global coordinates as

$$\mathbf{K} = \sum_{i=1}^{n} \left(k_i\frac{\partial L}{\partial \mathbf{q}}\frac{\partial L}{\partial \mathbf{q}^T} + k_i(L - L_0)\frac{\partial^2 L}{\partial \mathbf{q}\partial \mathbf{q}^T} \right)\Bigg|_{\mathbf{q}=\mathbf{0}} \tag{3.19}$$

To get rid of the state variables in the stiffness matrix, the computation is made as a linearisation around $\mathbf{q} = \mathbf{0}$. This stiffness method is compared with the previously calculated one and the results are identical. This is a good indication that the stiffness matrix is correctly calculated.

3.2.3 Numerical model in Adams View

The 3-DOF model depicted in figure 3.2 is implemented in the multibody dynamics simulation tool Adams View. The goal is to replicate the modal properties from the analytical solution to validate the model, and further on collect time domain data to compare the performance of different design set-ups. The Adams model can be seen in figure 3.4.

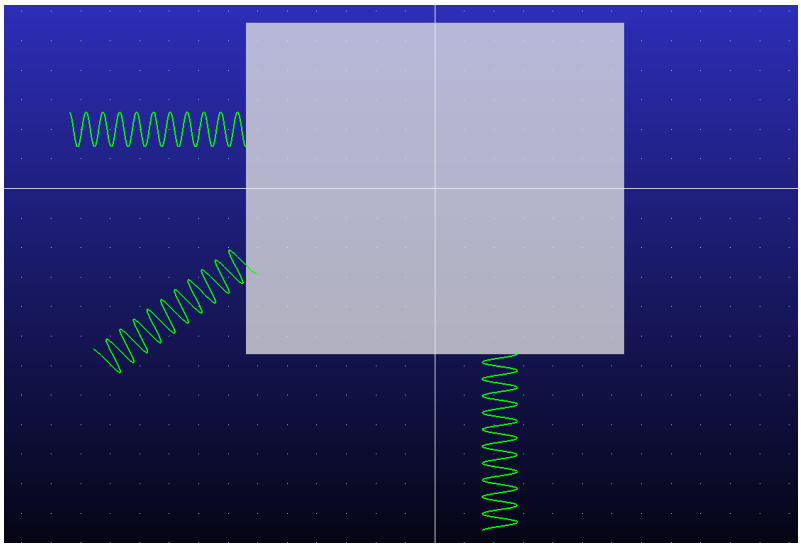

Figure 3.4: The 3-DOF model showed in Adams View.

According to the Adams view manual, spring-damper elements used in the picture above, perform badly when subjected to large deformations [8]. Since a wide range of design set-ups and load cases will be simulated, small oscillations cannot be guaranteed. To avoid this, a field element is implemented in the model containing the stiffness matrix from equation (3.11). This will replicate the behaviour of the springs without any concerns about the deformation magnitude. However, the spring-damper elements are used when validating against the analytical solution while the field element is used when executing different simulations.

3.2.4 Loading scenario

To execute the model in the time domain, initial conditions need to be applied. To correlate the model to an engine set-up, the load cases of interest are mainly pure rotation around the y-axis, corresponding to a rapid change of speed, and pure translation in z-direction, corresponding to running over an obstacle. However, the model was created in such way that it allows several general load cases to be applied. To translate these loading conditions into mathematical terms, they represent an impulse that excites the body. A strategy to implement the impulses in the model is to translate the loadings into initial

velocities. This can be done for forces and torques according to the law of momentum as follows

$$\mathbf{F}\Delta t = m\mathbf{v_0} \quad \Rightarrow \quad \mathbf{v_0} = \frac{\mathbf{F}\Delta t}{m} \tag{3.20}$$

$$T\Delta t = I\omega_0 \quad \Rightarrow \quad \omega_0 = \frac{T\Delta t}{I} \tag{3.21}$$

In the equations above, Δt represents the time duration of the impact which needs to be estimated for every force contribution. Doing this for every translational and rotational degree of freedom, an initial condition vector can be obtained by summing up the contribution from each loading. Adding this into the Adams model will generate a movement of the body, and since the system is undamped, the movement will continue forever.

3.3 6-DOF model

A three-dimensional model with a total of 6 DOFs was analysed both analytically and numerically. The DOFs consist of translation in x-, y- and z-direction along with rotation around all three axes. Unlike the 3-DOF model, this model was created to be more similar to an actual engine set-up used at VCC. The model consists of a rectangular rigid body and approximately four bushing elements representing the engine mounts that keep the engine in place. Another additional feature of this model is the ability to change the off-diagonal inertia terms. This makes it possible to represent how an additional mass component will influence the dynamic behaviour of the driveline system.

3.3.1 Analytical expressions of mass- and stiffness matrices

The mass matrix in a 6-DOF model is expanded compared to one for a 3-DOF model. The most obvious difference is the use of the inertia matrix to capture the rotational phenomena around every principal axis. The full mass matrix for a 6-DOF case can then be written as [18]

$$\mathbf{M} = \begin{bmatrix} m & 0 & 0 & 0 & 0 & 0 \\ 0 & m & 0 & 0 & 0 & 0 \\ 0 & 0 & m & 0 & 0 & 0 \\ 0 & 0 & 0 & I_{xx} & -I_{xy} & -I_{xz} \\ 0 & 0 & 0 & -I_{yx} & I_{yy} & -I_{yz} \\ 0 & 0 & 0 & -I_{zx} & -I_{zy} & I_{zz} \end{bmatrix} \tag{3.22}$$

where

$$I_{xx} = \frac{m\left(r_2^2 + r_3^2\right)}{3}, \qquad I_{yy} = \frac{m\left(r_1^2 + r_3^2\right)}{3}, \qquad I_{zz} = \frac{m\left(r_1^2 + r_2^2\right)}{3}$$

$$I_{xy} = I_{yx} = \int xy\,dm, \qquad I_{xz} = I_{zx} = \int xz\,dm, \qquad I_{yz} = I_{zy} = \int yz\,dm$$

In the 6-DOF model, the stiffness matrix becomes a 6×6 matrix. The expression for the matrix can be written as

$$\mathbf{K} = \begin{bmatrix} K_{11} & K_{12} & K_{13} & K_{14} & K_{15} & K_{16} \\ K_{21} & K_{22} & K_{23} & K_{24} & K_{25} & K_{26} \\ K_{31} & K_{32} & K_{33} & K_{34} & K_{35} & K_{36} \\ K_{41} & K_{42} & K_{43} & K_{44} & K_{45} & K_{46} \\ K_{51} & K_{52} & K_{53} & K_{54} & K_{55} & K_{56} \\ K_{61} & K_{62} & K_{63} & K_{64} & K_{65} & K_{66} \end{bmatrix} \tag{3.23}$$

where the indices 1, 2 and 3 represents the translational DOFs and 4, 5 and 6 represents the rotational DOFs. When finding the expression for the whole system's global stiffness matrix, the first step was to calculate it for one mount at the time. The local stiffness matrix for one mount consists of three translational stiffnesses and three rotational stiffnesses and can be expressed as

$$\mathbf{K}_{local} = \begin{bmatrix} k_{xx} & 0 & 0 & 0 & 0 & 0 \\ 0 & k_{yy} & 0 & 0 & 0 & 0 \\ 0 & 0 & k_{zz} & 0 & 0 & 0 \\ 0 & 0 & 0 & k_{\psi\psi} & 0 & 0 \\ 0 & 0 & 0 & 0 & k_{\theta\theta} & 0 \\ 0 & 0 & 0 & 0 & 0 & k_{\varphi\varphi} \end{bmatrix} \tag{3.24}$$

Since the rotational stiffnesses stay the same when changing the position of the mount, the transformation from local to global coordinates was only made for the translational stiffnesses. This means that when calculating the global stiffness matrix, only the 3×3 upper left part of $\mathbf{K}_{local}$, consisting of the translational DOFs, is used. Using a 3-1-3 rotation sequence for the angles α, β and γ gives the following rotation matrix for the 6-DOF model

$$\mathbf{A} = \begin{bmatrix} c(\alpha)c(\gamma) - c(\beta)s(\alpha)s(\gamma) & c(\alpha)s(\gamma) + c(\beta)c(\gamma)s(\alpha) & s(\alpha)s(\beta) \\ c(\gamma)s(\alpha) - c(\alpha)c(\beta)s(\gamma) & c(\alpha)c(\beta)c(\gamma) - s(\alpha)s(\gamma) & c(\alpha)s(\beta) \\ s(\beta)s(\gamma) & c(\gamma)s(\beta)s(\gamma) & c(\beta) \end{bmatrix} \tag{3.25}$$

where $c(x) = \cos(x)$ and $s(x) = \sin(x)$. By combining the total rotation matrix $\mathbf{A}$ and $\mathbf{K}^i_{local}$ according to equation (3.8), the global stiffness matrix for each mount i could be calculated. After $\mathbf{K}^i_{global}$ was determined, the spring forces could be decided according to equation (3.9), but now using following displacement vector

$$\mathbf{a} = \begin{bmatrix} x + \theta R_i(3) - \varphi R_i(2) \\ y - \psi R_i(3) + \varphi R_i(1) \\ x + \psi R_i(2) - \theta R_i(1) \end{bmatrix} \tag{3.26}$$

where $\mathbf{R}_i$ is the position vector of mount i, that now can be expressed as

$$\mathbf{R}_i = [r_x, r_y, r_z] \tag{3.27}$$

with r_x, r_y and r_z being the locations of the mount with respect to the global coordinate system. When the spring forces are calculated, the torques from the translational springs could be determined by using the same method as for the 3-DOF model, which can be found in equation (3.10). From here, the total global stiffness matrix $\mathbf{K}$ could be computed in the same way as described for the 3-DOF model, except that the rotational

stiffnesses from each mount were added to the diagonal terms K_{44}, K_{55} and K_{66}. By solving the eigenvalue problem in equation (2.4), the eigenfrequencies, ω and corresponding eigenmodes, Φ could be calculated.

3.3.2 Numerical model in Adams View

A numerical model of the 6-DOF system was implemented in Adams View. The model was not constrained in any direction which means that it is free to move as it wants. To replicate the stiffness attributes, a field element containing all stiffness elements from equation (3.23) was used. This means that no bushings were used, but the same behaviour was obtained anyway. However, bushing elements were used to validate the numerical model against analytical results. A model with four bushing elements is depicted in figure 3.5.

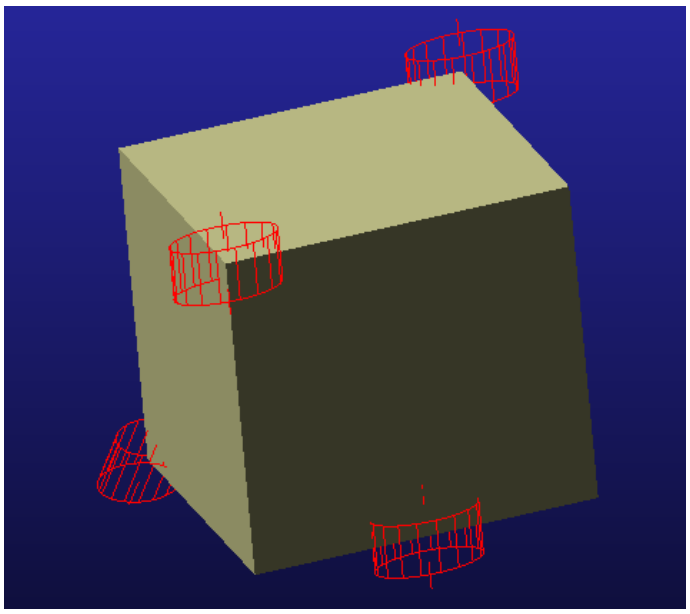

Figure 3.5: The studied 6-DOF model with four bushings showed in Adams View.

The forces and torques applied to the body are treated in the same way as in the two-dimensional case. This means that the impulses are converted to initial velocities applied to the centre of mass. For the translational DOFs, the velocities are calculated according to equation (3.20). However, for the rotational degrees of freedom, some more effort is needed. This is because the fact that the inertia matrix influences the dynamics of the body. The initial angular velocities can now be calculated as

$$\mathbf{T}\Delta t = \mathbf{I}\omega_0 \quad \Rightarrow \quad \omega_0 = \mathbf{I}^{-1}\mathbf{T}\Delta t \tag{3.28}$$

In practice, this means that even though a torque impulse is applied around a single axis, angular velocities will occur in the other directions as well due to the off-diagonal terms in the inertia matrix.

3.3.3 Loading scenario

What type of loading that the engine gets exposed to varies a lot and it can be both forces and torques. Since the dynamical behaviour of the body is load dependent, only one load has been investigated during this work. This makes it easier to compare the results and draw qualitative conclusions. The selected loading scenario became a torque impulse around the y-axis. This can for example be explained as a sudden speed increase of the engine. Another interesting loading could be force in z-direction, representing to drive on a bumpy road, but that is not covered in the scope of this thesis. The choice of loading scenario was decided in collaboration with VCC to be able to represent one of the most interesting events.

3.4 Verification of the models

The results from the two different models were verified by comparing the results from the analytical calculations in the Python script with the numerical results from the simulations in Adams View, using the same variable values for both analytical and numerical calculations. To make the verification, several different results were compared, including eigenfrequencies, eigenmodes and modal kinetic energy. For both the 3-DOF model and the 6-DOF model all those results became the same, but only the eigenfrequencies are presented here.

3.4.1 3-DOF model

When the verification for the 3-DOF model was made, translational springs were used instead of the field element, since the stiffness matrix in the field was taken straight from the analytical calculations. By showing that the results became the same for the analytical calculation and when using springs in the numerical simulation, the created 3-DOF model including the field element could be verified. In table 3.1, the eigenfrequencies from both the analytical calculation and the numerical simulation for an arbitrary set-up are listed from highest to lowest. As seen, they are identical.

Table 3.1: A verification showing that the eigenfrequencies became the same for both the analytical calculations and the numerical simulation in Adams for the 3-DOF model.

	Eigenfrequencies [rad/s]		
	ω_1	ω_2	ω_3
Analytical	214.4975	159.8724	26.1600
Numerical	214.4975	159.8724	26.1600

3.4.2 6-DOF model

The verification for the 6-DOF model was made with one bushing element. This means that three translational and three rotational stiffnesses were decided together with the position and orientation of the bushing. The way the analytical calculations were made

allows the user to add the wanted bushings one by one and then the same calculations are done for each bushing. Because of this, the verification of the model was accomplished by only using one bushing. When comparing the results of the modal quantities from both the numerical simulation and the analytical calculations, the results became the same. One example of the compared results are shown in table 3.2, where the eigenfrequency for each mode are listed from highest to lowest.

Table 3.2: A verification showing that the eigenfrequencies became the same for both the analytical calculations and the numerical simulation in Adams for the 6-DOF model.

	Eigenfrequencies [rad/s]					
	ω_1	ω_2	ω_3	ω_4	ω_5	ω_6
Analytical	338.9492	328.8753	141.4214	18.0608	7.7970	7.7445
Numerical	338.9492	328.8753	141.4214	18.0608	7.7970	7.7445

The eigenfrequencies from the analytical solution are identical to the ones from the numerical solution. This means that the implementation of a field element including the analytic stiffness matrix would provide the same results as the built-in bushings, which makes it much easier for the user to use the created Python script and create a DOE of a wanted set-up.

3.5 Variation of set-ups and data collection

Since the goal is to identify a modal quantity that can decide the driving experience, a wide range of set-ups need to be evaluated to obtain a full picture of the behaviour. Therefore, a routine is implemented in the Python script to try different set-ups and evaluate the given output data. The input parameters are varied with *Latin Hypercube Sampling* (LHS) mentioned in chapter 2.5. To be able to create a DOE by using LHS, the in-built function *lhs* from the Python package *pyDOE2* was used, to which the only two things needed are the number of wanted set-ups and design parameters. LHS takes the maximum and minimum value of each parameter and creates an evenly spread distribution of a number of set-ups that the modeller decides. The different input data that is needed is slightly different for the two models. In table A.1, all input variables that is required to be able to run the simulation of the 3-DOF model are listed.

Table 3.3: All input data needed to run the 3-DOF model.

	Input variable	Unit	Description
Body			
	r_1, r_2	[m]	Geometry of body
	m	[kg]	Mass of body
Springs			
	k_1, k_2, k_3	[N/m]	Spring stiffnesses
	a, b, c	[m]	Spring positions
	γ	[rad]	Spring orientation
Applied load			
	$\mathbf{F}$, Δt	[N], [s]	Force impulses
	$\mathbf{T}$, Δt	[Nm], [s]	Torque impulses

All properties under **Body** and **Springs** are shown in figure 3.2. The applied loads are used to be able to calculate the initial conditions. It is possible to add both forces and torques together with a duration time, Δt. To transform the impulses into initial conditions, equations (3.20) and (3.21) are used. The forces and torques are inserted as 3×1 vectors for each load and the number of separate applied loads are unlimited. The complete initial conditions are a combination of all loads.

To run the simulation for the 6-DOF model, a few more input parameters were needed, which are listed in table A.2. Equally as for the 3-DOF model, the torques and forces are added as vectors with a corresponding duration time. All parameters under **Bushings** are specific for each bushing, so if the wanted set-up consists of four different bushings, four sets of parameters are required. These are later combined to create the model's global stiffness matrix $\mathbf{K}$.

Table 3.4: All input data needed to run the 6-DOF model.

	Input variable	Unit	Description
Body			
	r_1, r_2, r_3	[m]	Geometry of body
	m	[kg]	Mass of body
	rot_x, rot_y, rot_z	[rad]	Orientation of body
Bushings			
	k_x, k_y, k_z	[N/m]	Translational stiffnesses
	$k_{\psi\psi}$, $k_{\theta\theta}$, $k_{\varphi\varphi}$	[Nm/rad]	Rotational stiffnesses
	x, y, z	[m]	Bushing position
	Rx, Ry, Rz	[rad]	Bushing orientation
Applied load			
	$\mathbf{F}$, Δt	[N], [s]	Force impulses
	T, Δt	[Nm], [s]	Torque impulses

The Python routine takes all drive cases and run them in Adams View. For every simulation, the output data is generated and stored before postprocessing. The output data collected from every simulation can be seen in table 3.5. Modal data and time domain data is saved together for each run.

Table 3.5: Output data collected from every setup.

Modal data	**Dimension, 6-DOF**
Modal kinetic energy	6×9
Matrix with eigenmodes	6×6
Eigenfrequencies	1×6
Participation factors	6×6
Time domain data	
RMS-value of displacement in every direction	1
RMS-value of velocity in every direction	1
RMS-value of acceleration in every direction	1
RMS-value of jerk in every direction	1
RMS-value of force in every direction	1
VDV in every direction w.r.t force	1

The root mean square (RMS) value is used to remove the sign dependency of the movement. For the time domain data, all the above mentioned are collected but not everyone is relevant for the work. The main focus is on the VDV in x-direction since that one is most equivalent to the comfortableness of the ride, and it is also a great measure for the smoothness of the ride in the longitudinal direction [12]. The other ones are collected mostly to find overall behaviour trends or if VCC will use the application for other purposes in the future.

3.5.1 Reordering modes

The output data in table 3.5 needs to be processed to be able to obtain useful information from it. From Adams View, the modes are ordered such that the one with the lowest corresponding eigenfrequency comes first and then in increasing order. However, for the modal kinetic energy and the participation factors it is essential that the modes are ordered such that the mode with most energy in x-direction comes first, followed by the one with the most energy in y-direction and so on. In that case, the matrices will be easier to compare with each other. An example of how the reordering can be done is seen in table 3.6.

Table 3.6: Reordering modes after dominant direction with respect to modal kinetic energy.

	Rx-mode	Y-mode	Ry-mode	Rz-mode	X-mode	Z-mode
X-DOF	0.46	2.72	0.47	9.93	**67.47**	18.95
Y-DOF	1.11	**92.94**	0.39	0.26	5.18	0.12
Z-DOF	0.01	0.75	20.27	0.00	14.01	**64.96**
Rx-DOF	**94.91**	1.45	0.67	2.74	0.00	0.23
Ry-DOF	0.64	1.07	**77.79**	1.44	4.30	14.76
Rz-DOF	2.87	1.07	0.41	**85.63**	9.04	0.98
Eigenvalue [Hz]	5.78	9.32	12.27	19.12	22.86	26.50

⇓

	X-mode	Y-mode	Z-mode	Rx-mode	Ry-mode	Rz-mode
X-DOF	**67.47**	2.72	18.95	0.46	0.47	9.93
Y-DOF	5.18	**92.94**	0.12	1.11	0.39	0.26
Z-DOF	14.01	0.75	**64.96**	0.01	20.27	0.00
Rx-DOF	0.00	1.45	0.23	**94.91**	0.67	2.74
Ry-DOF	4.30	1.07	14.76	0.64	**77.79**	1.44
Rz-DOF	9.04	1.07	0.98	2.87	0.41	**85.63**
Eigenvalue [Hz]	22.86	9.32	26.50	5.78	12.27	19.12

After reordering the modes, the eigenmode matrix and the modal kinetic energy matrix are immediately obtained. The post processing can then continue by also calculating the participation factor matrix that is described in chapter 2.2.2. In this way, all the modal data obtained from the Adams simulation is now stored in a way that makes it easier to compare a specific modal quantity between different set-ups.

3.5.2 Time domain data

To evaluate the performance of the model, the time domain data needs to be analysed as well. Since initial velocities are applied to the model, it will start to move. The simulation time is decided such that it is long enough to capture several full cycles and therefore

provide a full picture of the dynamic behaviour. From every simulation: displacement, velocity, acceleration and force in all directions are stored and processed. The data is taken from the centre of gravity which captures the behaviour of the full model well. Since the time data is unnecessary to store, the measurements are calculated as RMS-values. This generates a single value that describes the wanted output. However, it is important that the simulation time is sufficiently long to achieve proper results.

There are other interesting quantities that are not possible to extract directly from Adams, such as jerk and VDV. These are generated by using the other remaining data in the post-processing. Jerk is computed by differentiating the acceleration with respect to time and then converted into an RMS-value. VDV is a measurement of the force impact over time, more thoroughly explained in chapter 2.4. Both jerk and VDV are known to be good measurements of the comfort in a vehicle ride [11], which is why the extra effort is put to calculate those values as well.

To get sufficient time domain data, some effort was made to find proper solver settings in Adams View. This was done with the trial-and-error method until proper simulations were obtained. The problems arising with bad solver settings was that the movement of the body exploded or faded away. Since no damping were applied to the model, the movement should continue to infinity and not change magnitude after some cycles. The solver settings had to be more fine-tuned for the 3-DOF model since adding restriction in three out of six direction is computationally heavy.

3.5.3 Double modes

An interesting phenomenon is the behaviour of the system when two modes have similar eigenfrequencies, from now on called a double mode. The hypothesis is that design configurations with double modes will have a deviant behaviour from the rest. To detect configurations with double modes, the difference between two adjacent modes is compared. If the difference is lower than a certain value, the design is considered to contain a double mode. Note that in theory, a double mode is defined as two eigenmodes with identical eigenvalues, but in numerical solutions, that would rarely happen.

3.6 Statistical correlations

When the data is stored and all requested quantities are obtained, the data needs to be analysed in order to draw conclusions of the performance regarding vibration isolation. Different methods are conducted to finally obtain a quantitative measure in the modal domain that can augur something about the time domain behaviour.

3.6.1 Reference value

In order to decide whether a setup performs well or bad, a reference value is needed. At VCC, one of the commonly used performance indices is the VDV in x-direction, i.e. the driving direction. Lowering this value will increase the comfort experience for the occupants in the vehicle. To obtain a reference value for a specific load case, VCC uses a

certain percentage of the modal kinetic energy in Ry-direction for the most x-dominant mode. Doing this for a set of design configurations, a reasonable limit for the VDV can be obtained. This is used to categorize every setup as a *good* setup or a *bad* setup. To find the wanted reference value, a large DOE was created of an already existing set-up. The parameter values were allowed to vary between $\pm 50\%$ of the original value, which makes it possible to create a lot of different combinations of the original set-up. The number of samples was set to 10 000. The obtained value from this DOE was later used as reference value for every run.

Note that when using this method, the reference value is load dependent. This means that the loading scenario needs to be the same to be able to compare the results between different DOEs. As applied load, a torque around the y-axis was used with a magnitude of 200 Nm and a duration time of 10 ms.

3.6.2 Correlation matrices and scatter plots

The next step is to compare the modal data with respective time performance. To visualise the trends and correlations, scatter plots as the one seen in figure 3.6 are studied. These types of plots are a great tool for obtaining an overview on how well a modal quantity agrees with a specific time domain data. They are also good to find the range between the lowest and highest value of a quantity.

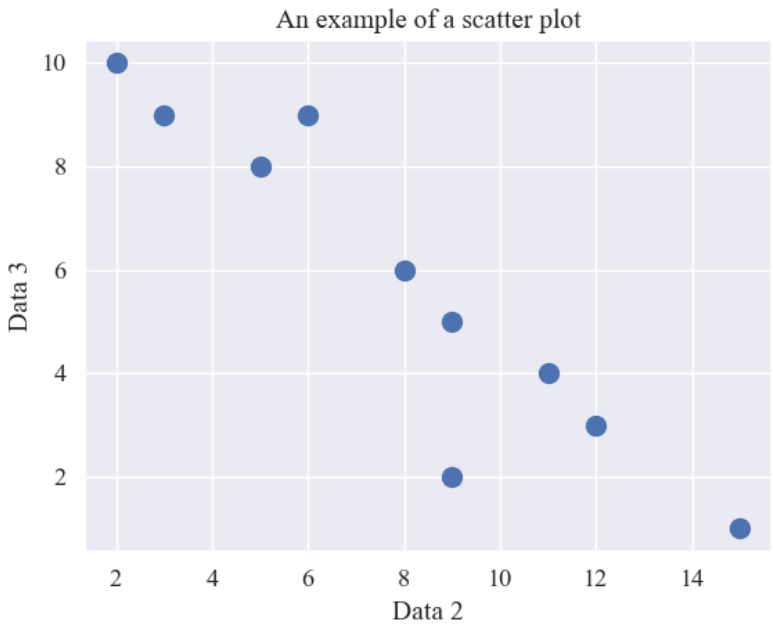

Figure 3.6: An example of a scatter plot over two data sets.

To get an overview of how all possible quantities correlate, a correlation matrix is computed. There are different correlation numbers that can be used to measure the relationship between data sets. This study uses Spearman's rank correlation which is more thoroughly described in chapter 2.6. An example of a correlation matrix can be seen in figure 3.7. An

absolute value close to one means a high correlation while a value close to zero means no correlation at all. Negative values implies that an increase in x means a decrease in y.

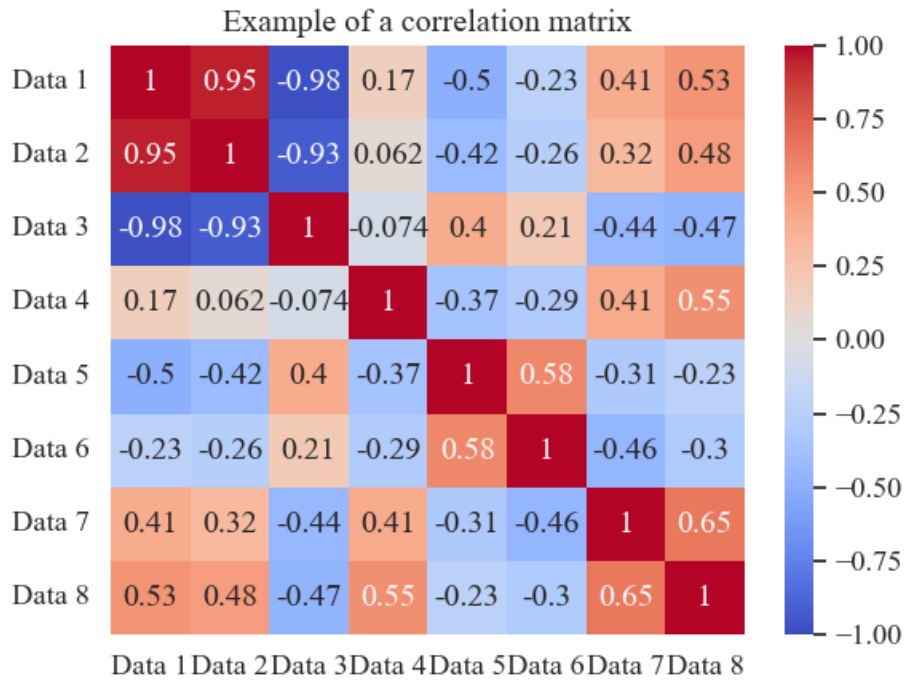

Figure 3.7: An example of a correlation matrix with Spearman's rank correlation.

When comparing the data in figure 3.6 with the correlation matrix above, it indicates that it has a Spearman's rank correlation of -0.93. This seems accurate since the graph shows a decreasing trend with high correlation according to the naked eye. This shows the strength of scatter plots, to evaluate the correlation coefficient with an engineering judgement.

In this thesis, there are many quantities to compare. Since the interesting comparison is between time domain data and modal domain data, there are no need to visualize the full correlation matrix. The matrix will therefore be divided into submatrices only showing time domain data vs. modal domain data.

4

Results

In this chapter, the result of the work is presented. Both results from the 3-DOF and 6-DOF model are obtained and analysed. However, the 6-DOF model is the most realistic one and if any conclusions are presented, they are due to the results from that model if nothing else is mentioned. Several runs have been made with different set-ups and different range of parameter variation. All investigations will be presented in this chapter and together they will be used to draw conclusions on the dynamical behaviour and sensitivity of parameter change.

4.1 Analysis of 3-DOF model

The two-dimensional model with three DOFs was simulated in Adams View. The variation of parameters was arbitrary, but the nominal values was in the same size order as in an electric driveline installation. The maximum and minimum values of each design parameter are shown in appendix A. The initial conditions of the model are equivalent to a torque impulse around the y-axis with a magnitude of 200 Nm under a duration of 7 ms. This resulted in a correlation matrix that can be seen in figure 4.1. In the figure, k stands for stiffness, p is participation factor and E is modal kinetic energy. The indices 1, 3 and 5 indicates direction x, z and Ry. For p and E the first index indicates the modal direction, and the second index tells which direction that is the most dominant in that specific mode.

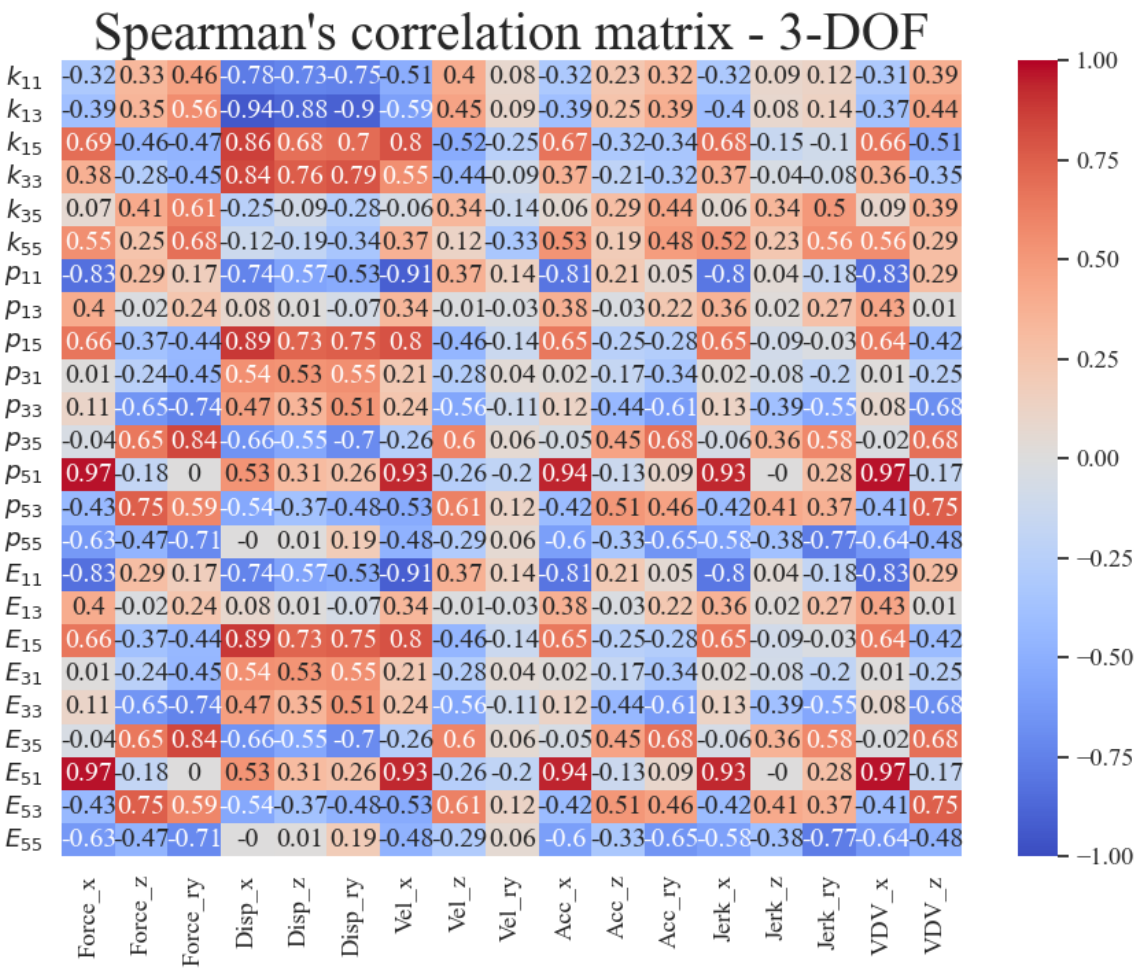

Figure 4.1: Spearman's rank correlation between modal and time quantities for the 3-DOF model.

The modal quantities with the highest Spearman's correlation for the most interesting time domain quantity (VDV in x-direction) is p_{51} and E_{51}. In fact, the modal kinetic energy and participation factor shares the same value for every direction. This is because in a two-dimensional model participation factor and modal kinetic energy are the same, as mentioned in section 2.2.4. A scatter plot of every design's correlation between VDV in x-direction and modal kinetic energy in Ry-direction for the most x-dominant mode can be seen in figure 4.2. This shows a high correlation between the two quantities.

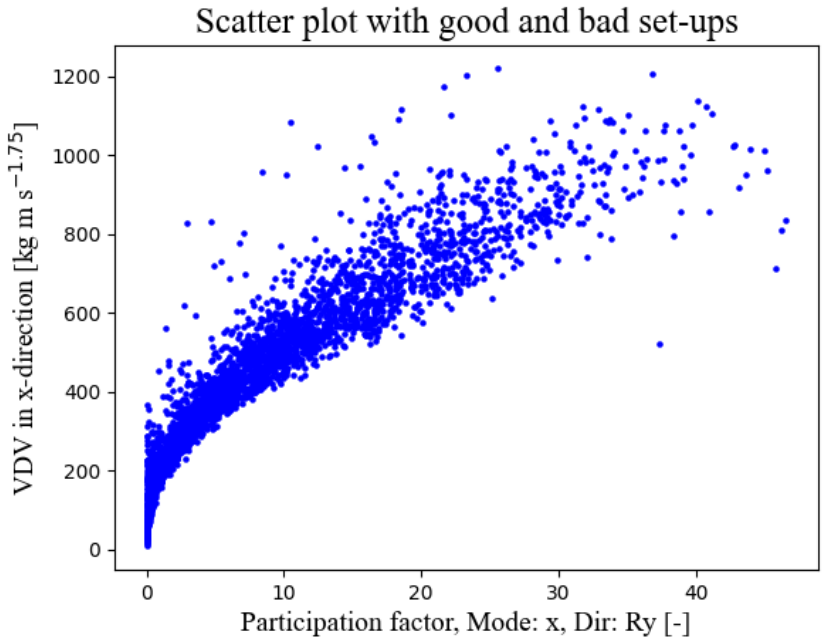

Figure 4.2: Scatter plot showing the correlation between one modal- and one time quantity, $\rho = 0.97$.

The results from the 3-DOF model are mainly used to get an understanding of the expected outcome from the 6-DOF model. It is also used to detect errors and help developing the more complex three-dimensional model. This means that no further analysis on modal requirements have been done for this model.

4.2 Analysis of 6-DOF model

The 6-DOF model was analysed for simulations with different intentions. Firstly, a large variation was performed to get an overview of the complete spectrum of possible set-ups. This run was used to find a reference value according to earlier knowledge at VCC. Since there are no interest to analyse very bad performing configurations, two smaller LHS samples were made as well; one with design parameters close to a well performing set-up and one with parameters close to a set-up with a VDV close to the reference value. In addition, the influence of inertia properties was also investigated.

4.2.1 Reference value

To be able to use the same reference value for all the created runs, an already existing and known set-up was used. The values of the design parameters are listed in appendix A for reproducibility. By letting the values of the design parameters vary with $\pm 50\%$, a reference value could be found. The reference value was taken from the scatter plot that are presented in figure 4.3 and the result became a VDV_x of 530 kg m s$^{-1.75}$. This was from now on used as a limit to divide the set-ups from every run with the 6-DOF model as *good* or *bad*, where the good ones are the set-ups with a VDV lower than the limit and the

bad ones are the set-ups with a VDV higher than the limit. The selected reference value was the lowest existing VDV in the plot to have a higher modal kinetic energy in the *x*-mode in *Ry*-direction than the used requirement allowed. Due to confidential information, the values on the *x*-axis are hidden.

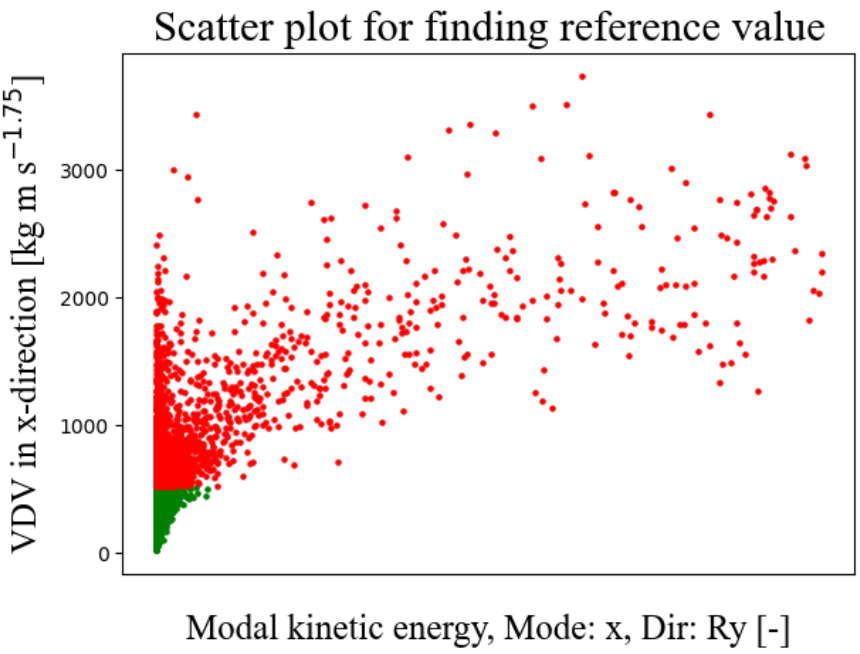

Figure 4.3: Scatter plot that was used to find the reference value which later on was used to decide whether a design was *good* or *bad*, $\rho = 0.45$.

Out of the 10 000 different designs in this run, 8045 ended up as *good* set-ups, which is around 80%. The number of good designs was not equally high for the other created runs, since the "start" design not always was such a good set-up and it also depends on how much the design parameters are allowed to vary during the DOE. How this changes depending on which set-up is used will be further investigated in the upcoming sections.

4.2.2 Complete LHS

The complete LHS created to find the reference value was used for further investigation. To ensure that the parameters were independent of each other, the correlation between them was calculated and can be seen in figure 4.4. This shows that the only terms that correlates with each other are the inertia terms. This is not strange since inertias are calculated properties from the mass and geometry, according to equation (3.22) and not decided by the modeller.

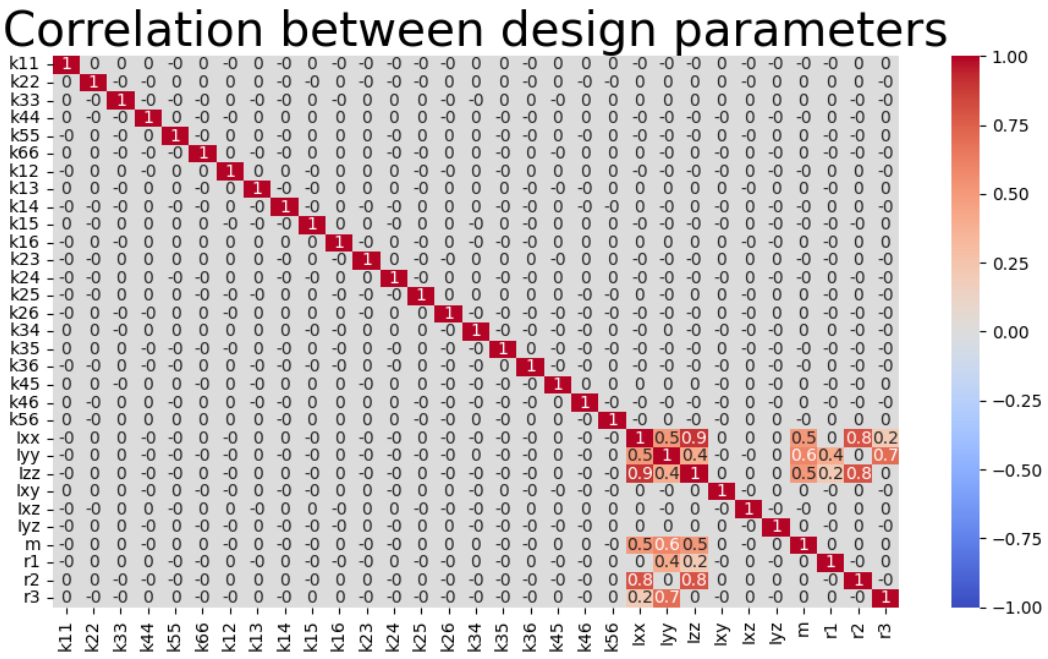

Figure 4.4: The correlation between design parameters to evaluate the performance of the LHS.

A Spearman's correlation matrix was obtained for this run of set-ups. Since there are a lot of quantities to compare it was hard to visualize them in a single matrix. Therefore, the data was categorized into different correlation matrices which can be found in appendix B. The highest correlation for VDV in x-direction is found for E_{15} and p_{15}, i.e. modal kinetic energy as well as participation factor in the Ry-dominant mode in x-direction with a value of $\rho = 0.8$. The latter one is showed in figure 4.5.

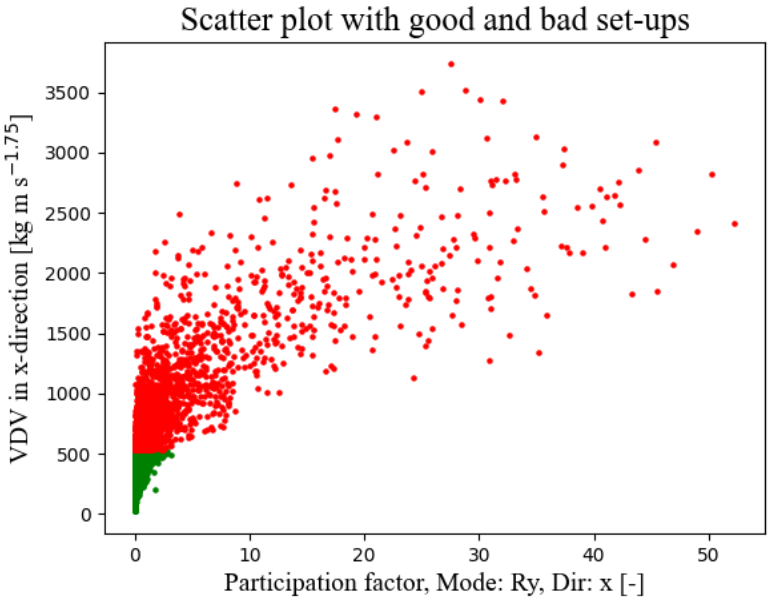

Figure 4.5: Scatter plot of the modal quantity with the highest correlation to VDV in x-direction, $\rho = 0.8$.

The plot shows that the higher the modal quantity, the higher the VDV value. However, a low modal quantity does not guarantee a good performance since many configurations have high VDV values despite having a low modal quantity. Another interesting discovery from this run is that some configurations have p_{15} values around 50%, which is strange since the mode is told to be dominant in *Ry*-direction and therefore should not have such a high movement in *x*-direction. This indicates the inherent difficulty in the reordering of the modes which will be discussed more in chapter 5.1.1.

4.2.3 Difference between well- and bad performing set-ups

A question that arises is if there are any major differences in input parameters between a well- and bad performing set-up. The differences in VDV can for some modal quantities differ significantly for the same value on time domain requirement. Taking a glance at figure 4.3 that uses the previous requirement at VCC as x-axis, there is a major variation in VDV for a modal quantity close to zero. To dig deeper into this, two set-ups are picked from that figure; one with a low VDV and one with a high VDV but both with the modal quantity close to zero. The two chosen designs are highlighted in figure 4.6.

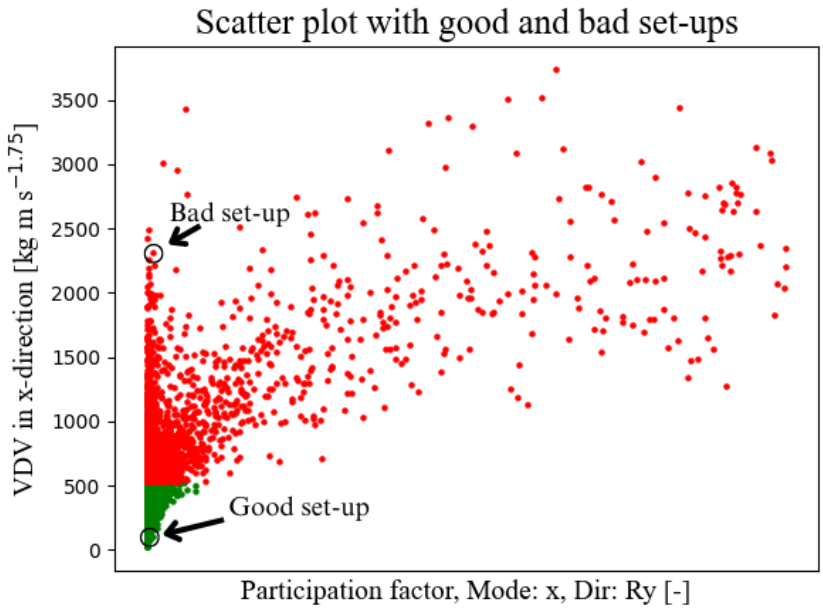

Figure 4.6: Two chosen set-ups to compare time history data between one *good* and one *bad* set-up.

Running these configurations in Adams View gives the time history for force in *x*-direction according to the graphs in figure 4.7. As observed, the peak value of the force for the poorly performing design is around ten times higher than for the well performing one. When analysing the input variables, the major differences between the two set-ups are the terms that influences the inertia matrix, both the diagonal and off-diagonal terms, i.e. the mass, dimensions and orientation of the block.

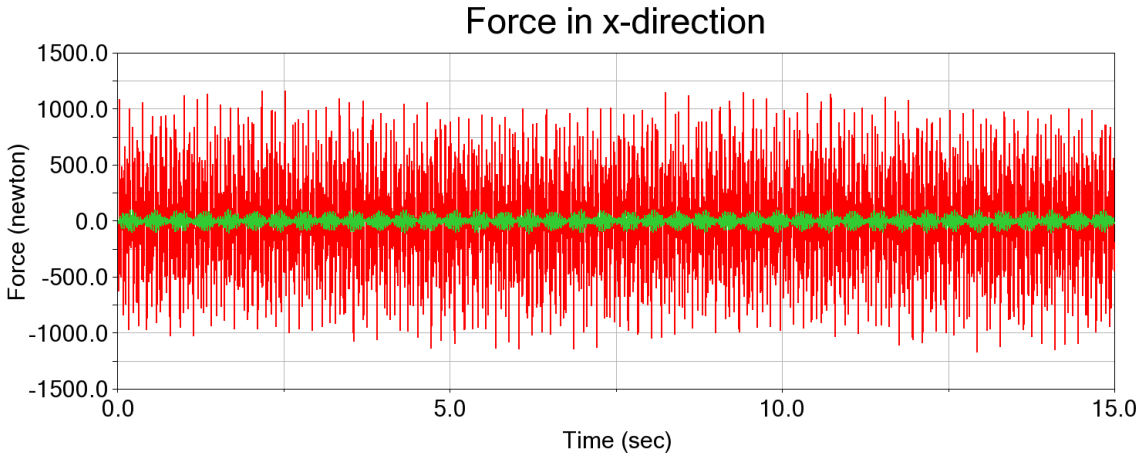

Figure 4.7: The time history of force in x-direction for two set-ups. The red one performs bad and the green one performs well.

To visualize the difference in the inertia matrix, the quotient for each term between the *good* and *bad* set-up was calculated. This resulted in the following matrix

$$I_{good/bad} = \begin{bmatrix} 8.31 & 3.42 & -2.89 \\ 3.42 & 2.82 & -15 \\ -2.89 & -15 & 9.79 \end{bmatrix} \tag{4.1}$$

All terms in the matrix shows that the magnitude of each term is larger for the *good* set-up compared to the *bad* one. From equation 3.22, it is possible to find out that the reason why the diagonal terms are larger for the *good* set-up is because of greater products between mass and the dimensions of the body. The off-diagonal terms are mainly influenced by the orientation of the body.

4.2.4 Influence of inertia properties

To gain more knowledge of how the interesting parameters influence the result, new simulations were made. In these simulations, the physical parameters influencing the inertia were the only ones allowed to vary. This includes dimensions of the block, body mass and orientation of the block. All simulations were done with 200 samples. In the upcoming scatter plots, the modal requirement that performed best in the complete LHS is used on the x-axis.

4.2.4.1 Variation of diagonal inertia terms

The diagonal terms in the inertia matrix depends on geometrical properties and the mass of the body. When letting the rotation of the body be zero in all directions, only the diagonal terms are non-zero. Doing a simulation when only varying the dimension of the block in all directions with $\pm 50\%$, the scatter plot seen in figure 4.8 is obtained. The range of the VDV is ≈ 850 kg m $s^{-1.75}$, which is a large variation. However, it should be mentioned that most of the set-ups perform well and are gathered in the bottom left corner of the figure.

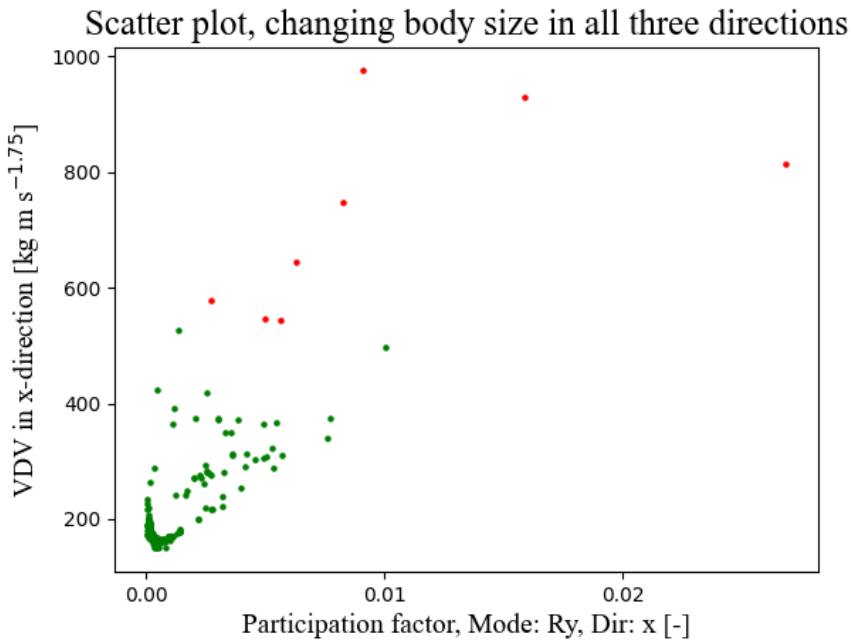

Figure 4.8: Scatter plot of VDV in x-direction vs. participation factor in mode Ry in x-direction for set-ups when allowing variation of body size in all three directions, $\rho = 0.37$.

To gain a better understanding of the influence of the different dimensions, each one is varied at the time. Figure 4.9 shows how each dimension influences the dynamic response of the model. In figure 4.10, two zoomed in pictures are shown for the lowest values when varying r_2 and r_3 for a better visualization.

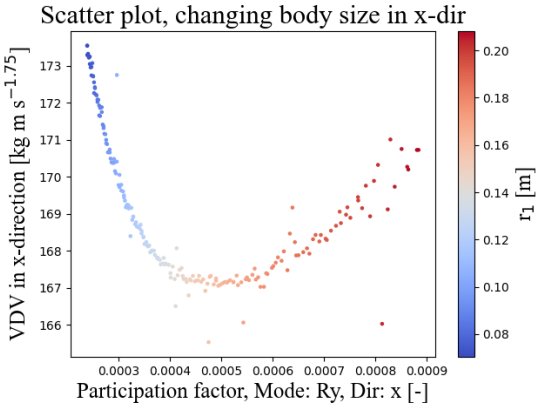

(a) Changes in x-direction, $\rho = -0.59$.

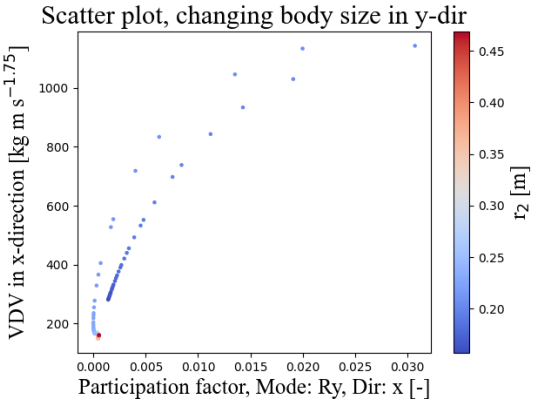

(b) Changes in y-direction, $\rho = 0.11$.

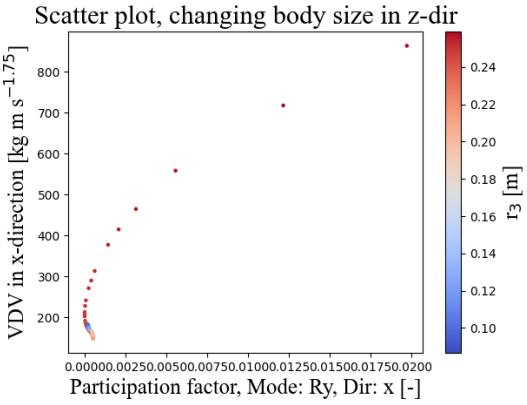

(c) Changes in z-direction, $\rho = -0.77$.

Figure 4.9: Plots showing how changes in body size in one direction at the time affects the VDV_x vs. participation factor in the *Ry*-mode in *x*-direction.

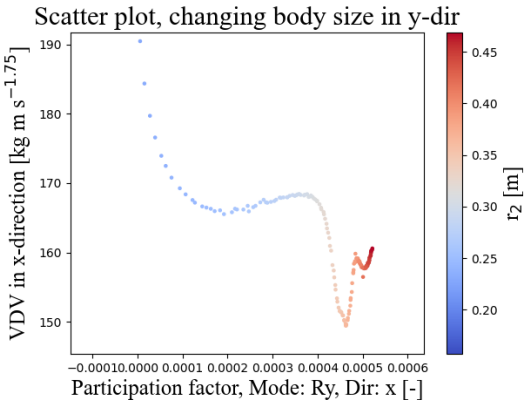

(a) Changes in y-direction, zoomed in, $\rho = 0.11$.

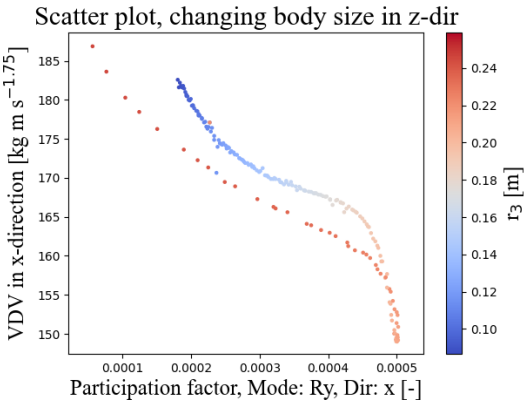

(b) Changes in z-direction, zoomed in, $\rho = -0.77$.

Figure 4.10: Zoomed in plots showing how changes in body size y- and z-direction effects the VDV_x vs. participation factor in the *Ry*-mode in *x*-direction.

The figures show a behaviour where a clear optimum is obtained to lowering the vibra-

tions that the occupants perceive. It can also be seen that the sizes in y- and z-direction influence the VDV much more than the size in x-direction. It shows that for this specific load case, a decrease in r_2 and an increase in r_3 means a lower comfort for the occupants in the car.

Another difference between the well- and bad performing set-ups compared in section 4.2.3 was the mass of the body. To investigate how the mass affects the final set-up, a DOE when only the mass changed was done, all other design parameters were kept constant. To have something to compare the results with, another run were allowing variation with $\pm 50\%$ in both body size and mass was created. The results from both the run where the body size and mass and the one when only the mass changed is presented in figure 4.11.

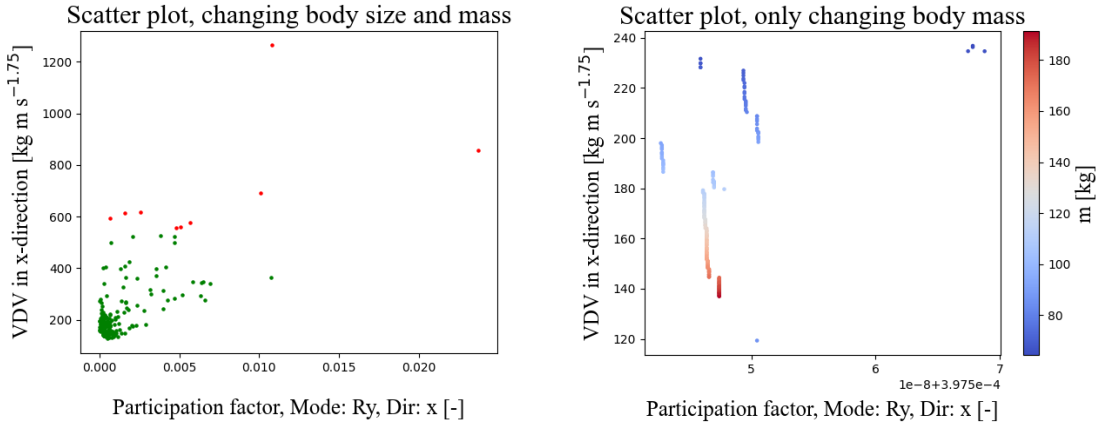

(a) Changes body size in all directions as well as the mass, $\rho = 0.36$.

(b) Only changes body mass, $\rho = -0.02$.

Figure 4.11: Plots showing how changes in body size in all directions and mass effects the VDV_x vs. participation factor in the Ry-mode in x-direction.

There are similarities in behaviour between figure 4.8 and 4.11a, which means that the mass does not affect the results that much. This is confirmed when comparing figure 4.8 with the scatter plot when only the mass is allowed to change, figure 4.11b. From that comparison, it is obtained that changes in mass almost does not affect the participation factor at all and an increase in body mass only results in a decrease in VDV_x.

4.2.4.2 Variation of off-diagonal inertia terms

The inertia matrix of the model is also influenced by changing the orientation of the rigid body. By changing the orientation, such that the principal axes of the system no longer coincide with the axes of the global coordinate system, off-diagonal terms in the inertia matrix will be created. This also affects the global mass matrix that is presented in equation (3.22). To be able to study the influence of the off-diagonal terms in the inertia matrix, a simulation only allowing the rotation of the body to change was made. The three rotations rot_x, rot_y and rot_z, presented in table A.2, were allowed to vary in the span $[-\pi/40, \pi/40]$, while all other parameters were fixed with the same values as the ones used in the large 10 000 samples run. In figure 4.12, one of the results from the simula-

tion is presented. It shows a large variation of VDV in x-direction even though everything except the inertia matrix is kept constant for each design.

Even though the participation factor on the x-axis barely varies, the behaviour of the curve is interesting. The range of the VDV is ≈ 150 kg m s$^{-1.75}$, while the chosen participation factor only changes from ≈ 0 to 0.002, which means that small changes in participation factor results in large changes in VDV$_x$.

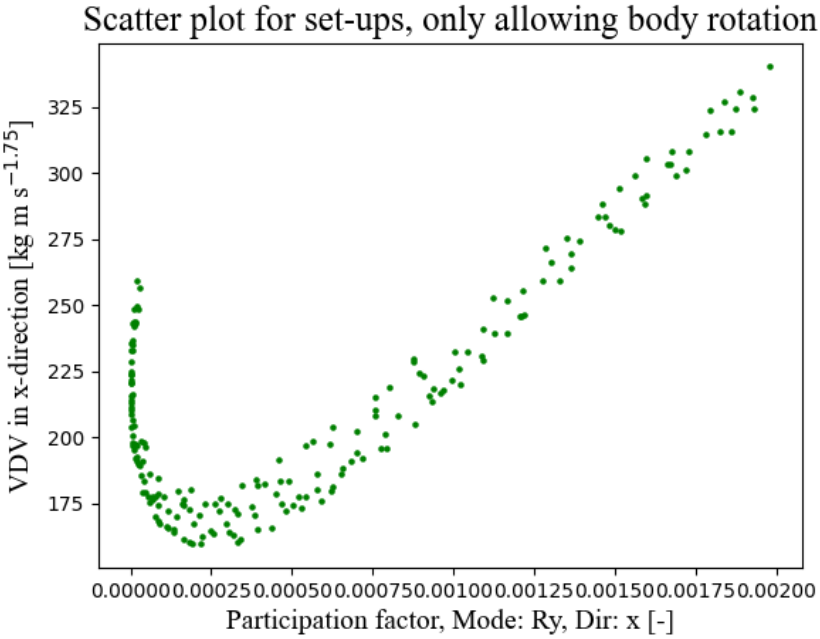

Figure 4.12: Scatter plot of VDV in x-direction vs. participation factor in mode x in Ry-direction for set-ups when allowing body rotation in all three directions, $\rho = 0.46$.

Since the 6DOF-model consists of three different rotational DOFs, all three rotations contribute to the behaviour presented in figure 4.12. To understand how the different contribution from each DOF affects the mixed behaviour, three different runs were created where only one rotation was allowed in each run. All design parameters were kept constant except from one of the rotations, which was allowed to rotate in the span $[-\pi/40, \pi/40]$. All the three different behaviours can be seen in the plots in figure 4.13.

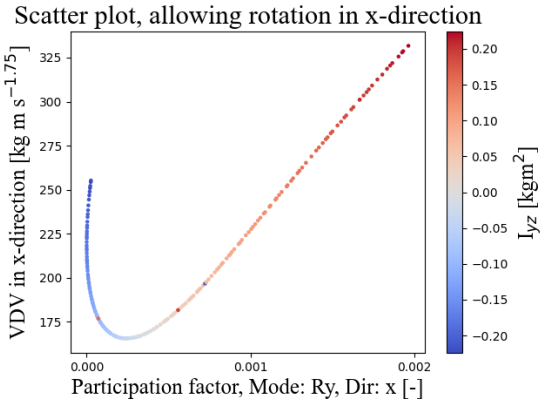

(a) Rotation only about x-axis, $\rho = 0.45$.

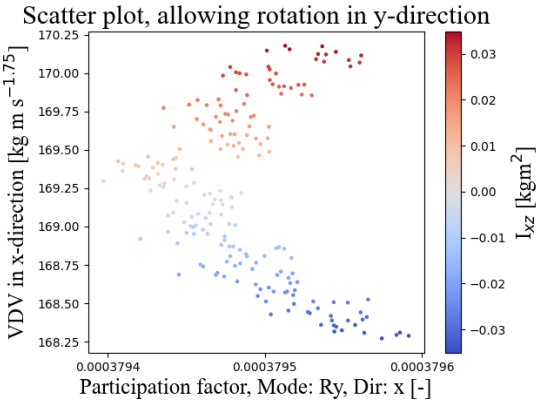

(b) Rotation only about y-axis, $\rho = 0.2$.

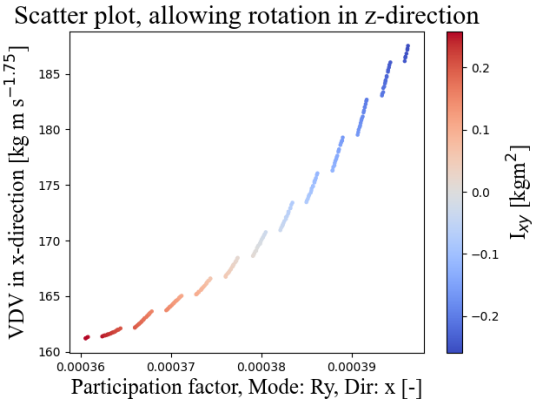

(c) Rotation only about z-axis, $\rho = 1$.

Figure 4.13: Plots showing how rotation about only one axis at the time effects the VDV_x vs. participation factor in the *Ry*-mode in *x*-direction.

The most obvious result from the figures is that the only plot with the same behaviour in both VDV and participation factor as figure 4.12 is the plot with rotation in *x*-direction, figure 4.13a. It is only for this plot where the lowest VDV coincide with no rotation, since the inertia term I_{yz} only appears when having a rotation around the x-axis. For both figure 4.13b and 4.13c the lowest VDV appears somewhere in the middle. By only study these three plots, the result would be that it is the rotation around the x-axis that affects the overall behaviour the most.

4.2.5 Variation of a set-up close to reference value

Since the complete LHS showed a wide spread of performances, more narrow runs were made to find better trends. One interesting idea is to see how variations of set-ups close to the reference value affect the performance of the model. In figure 4.14 the configurations closest to the target value are shown with respect to the old requirement used at VCC. This is a zoomed in picture of figure 4.3 with a VDV of $\pm 10\%$ around the reference value. Four set-ups are marked in the figure. Those were chosen as starting points for the narrow simulations.

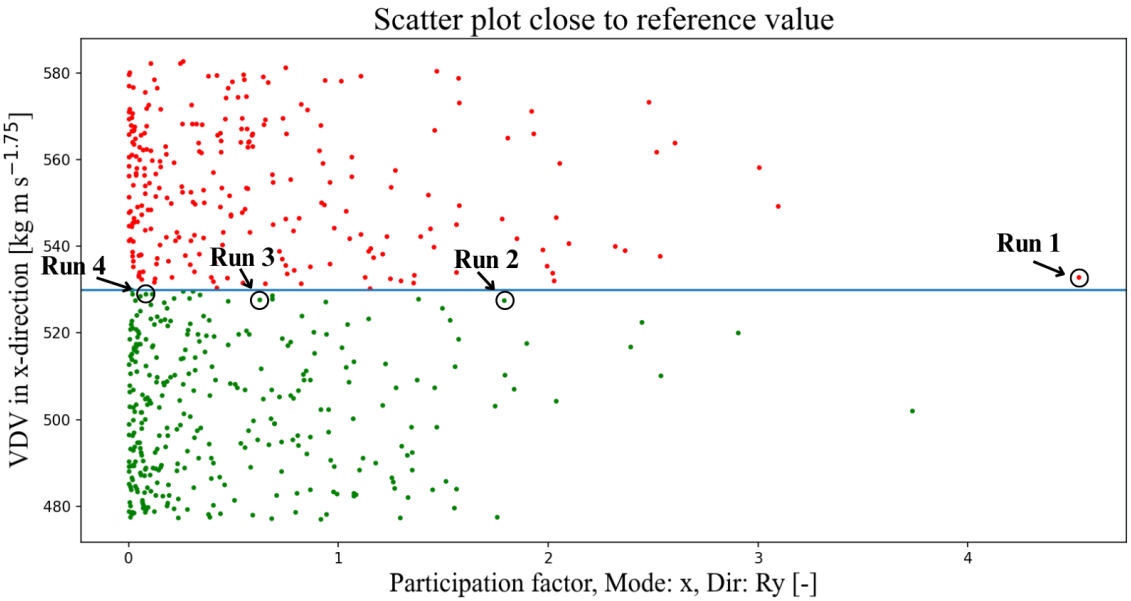

Figure 4.14: Scatter plot of all designs within $\pm 10\%$ of the reference value.

The four marked configurations in the figure above were simulated with a variation of the design parameters of $\pm 1\%$. 2500 samples were generated for each run. One modal quantity with high correlation for each run was participation factor in x-mode for the Ry-direction, which is depicted in figure 4.15. In table 4.1, some interesting information from the scatter plots is collected in numbers.

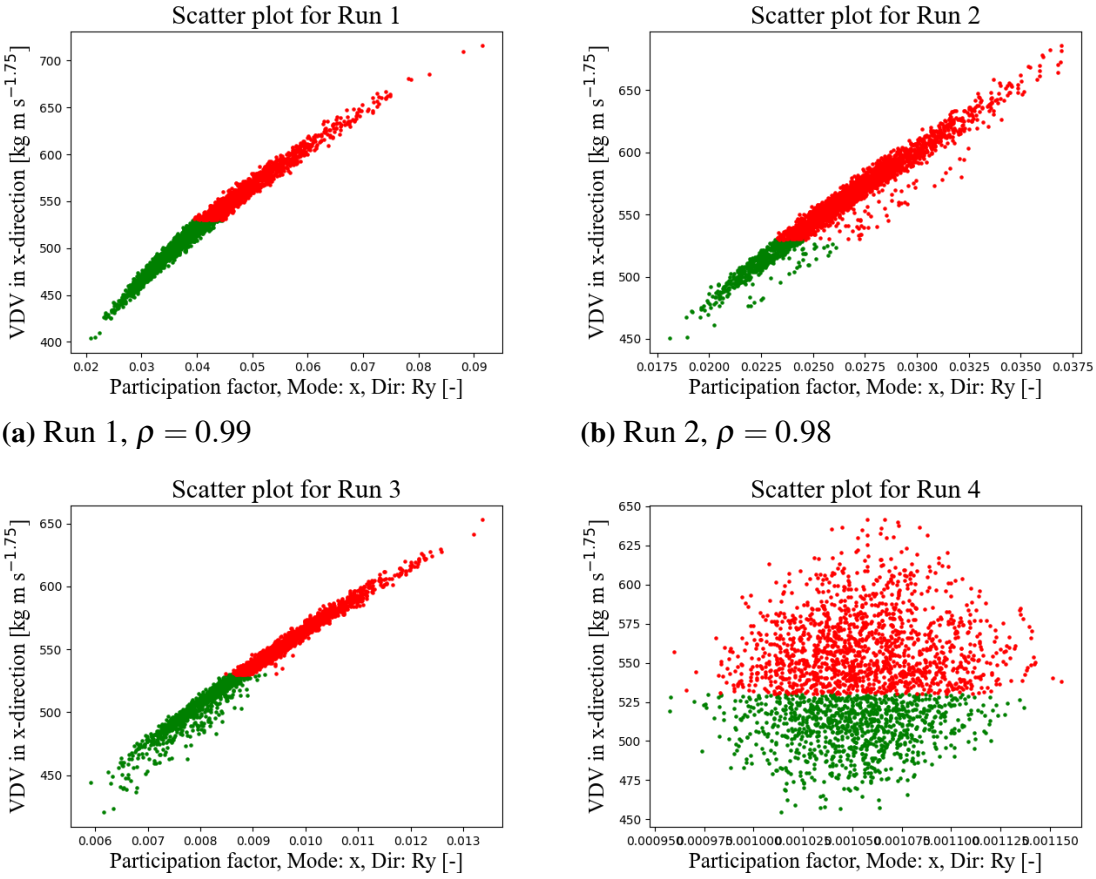

(a) Run 1, $\rho = 0.99$

(b) Run 2, $\rho = 0.98$

(c) Run 3, $\rho = 0.99$

(d) Run 4, $\rho = 0.09$

Figure 4.15: The correlation between participation factor for mode x in Ry-direction and VDV in x-direction for four different runs close to the reference value.

Table 4.1: Comparison of the runs close to the reference value.

	Percentage of good set-ups	**Lowest VDV_x [kg m s$^{-1.75}$]**	**Highest VDV_x [kg m s$^{-1.75}$]**	**Range of VDV_x [kg m s$^{-1.75}$]**
Run 1	54%	404	716	**312**
Run 2	20%	450	686	**236**
Run 3	45%	421	653	**232**
Run 4	41%	454	641	**187**

The things that can be concluded from figure 4.15 and table 4.1 is that when lowering the old requirement, the VDV in x-direction lowers its peak even though the same variation in distribution has been made. Also, the range between the highest and lowest value of VDV decreases together with this requirement. However, there is not easy to say anything about the number of approved set-ups and the sensitivity in parameter change but the trends are the same in all places of the distribution close to the reference value.

In figure 4.15d, the trend does not look like the trends in the other three runs. This may depend on the maximum difference of $2 \cdot 10^{-4}$ on the x-axis, which may make it hard to distinguish the runs from each other. It is worth mentioning that figure 4.15 only shows one specific modal quantity. This quantity had a high correlation for run 1-3 but low for run 4. However, run 4 have high correlations on other modal quantities and should still be considered as a valid simulation.

4.2.6 Variation of a good set-up

Another run that was created was the one made from one of the best configurations in the 10 000 samples run. This means one of the configurations with both the lowest VDV and lowest modal kinetic energy according to the used requirement. All design parameters were allowed to vary with $\pm 1\%$ from the original values and in total 2500 different designs were sampled. To be able to understand if a good design behaves in the same way as the configuration mentioned in section 4.2.5, the same modal quantity was compared for this run as well, which resulted in figure 4.16.

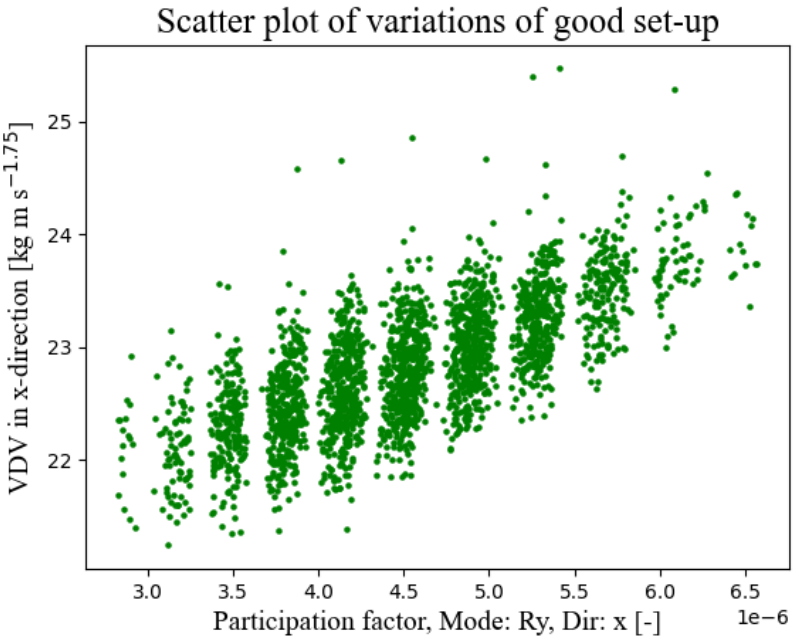

Figure 4.16: Scatter plot of small variations around one of the best designs from the earlier presented run with 10 000 samples, for VDV in x-direction vs. participation factor in the Ry-mode in x-direction, $\rho = 0.72$.

The plot shows that the behaviour is similar as for the configuration close to the reference value, but the changes in VDV is not equally high for the run of a good configuration, even though the parameters were allowed to vary equally much in both runs. Figure 4.16 presents an interesting pattern for how the participation factor in mode Ry in direction x varies. The difference between the highest and lowest value is so small that small differences in the already small span cannot be detected because of the error tolerance from the

simulations in Adams. This is the reason to the striped pattern in the figure.

Neither the difference between the highest and lowest VDV is equally high as for the run close to the reference value. In figure 4.16 the VDV varies from ≈ 21 kg m $s^{-1.75}$ to ≈ 25 kg m $s^{-1.75}$, which gives the quotient of 1.19 between the highest and lowest value, which is much lower than the range presented in table 4.1. In that case, the quotient varies between $1.41 - 177$. This means that the range between VDV is much lower when varying the good set-up even though the variation is the same of $\pm 1\%$. This gives the conclusion that a *good* set-up is less sensitive to change than a *bad* set-up.

4.2.7 Combinations of modal quantities

An interesting idea is that combinations of modal quantities may provide good information about the performance regarding vibration isolation, i.e. good correlation with VDV in x-direction. The quantities to be tested are the ones that perform well on their own as well as combinations that VCC has had in mind before. Since the applied load in this case is a torque impulse around the y-axis and the sensitive direction for vibration isolation is x-direction, the coupling between these modes will be prioritized. In table 4.2, the combinations that have been tested are listed. The last combination in the table is the one that Longoni assumed was the best in the previous work done at VCC in 2020 [3].

Table 4.2: Combinations of set-ups that were tested.

$E_{15} \cdot E_{51}$
$p_{15} \cdot p_{51}$
$\sum_{i=1}^{6} E_{1i} \cdot E_{5i}$
$\sum_{i=1}^{6} p_{1i} \cdot p_{5i}$
$\delta E_{15} + (1-\delta) E_{51}$
$\delta p_{15} + (1-\delta) p_{51}$
$-1250 p_{55} \cdot p_{15} + 75.05$

One of the tested combination is a linear combination between the two before mentioned quantities with $\delta \in [0,1]$. This is done for both modal kinetic energy and participation factor. The scalar factor δ is varied to see which value that generates the highest Spearman's rank correlation. For both *Modal kinetic energy* and *Participation factors*, this occur when $\delta \approx 77\%$ as seen in figure 4.17. This means that as requirement, the modal participation for *Ry*-mode in x-direction affects the most, which is opposite to what VCC has used before. The value obtained for δ will be used in further comparison.

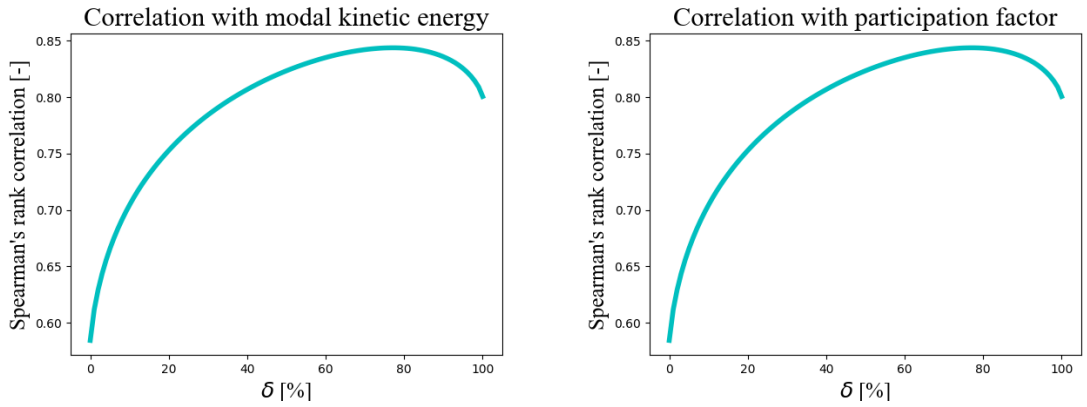

(a) Modal kinetic energy **(b)** Participation factor

Figure 4.17: Varying δ to see which combination that gives the highest Spearman's rank correlation.

The combinations from table 4.2 are evaluated for four different simulations; the complete LHS, the set-ups from the complete LHS closest to the reference value, *Run 1* from chapter 4.2.5 and when varying a well performing set-up. The factor δ is put as 0.77 accordingly to the findings in the figure above. The Spearman's rank correlation for all these cases can be seen in table 4.3. For comparison, the quantities used in the combinations are presented alone to see the improvement of these requirements. The conclusion is that in general, the combined modal quantities perform better than when being alone.

Table 4.3: Spearman's rank correlation for every combination for different simulations as well as the best performing single quantities.

	Complete LHS	**Ref-val** $\pm 10\%$	**Run 1**	**Good set-up**
E_{15}	0.80	0.12	0.98	0.72
p_{15}	0.80	0.12	0.98	0.72
E_{51}	0.58	0.05	0.99	-0.45
p_{51}	0.45	0.07	0.99	-0.44
$E_{15} \cdot E_{51}$	0.77	0.10	0.99	0.17
$p_{15} \cdot p_{51}$	0.62	0.10	0.99	0.84
$\sum_{i=1}^{6} E_{1i} \cdot E_{5i}$	0.85	0.13	1	0.30
$\sum_{i=1}^{6} p_{1i} \cdot p_{5i}$	0.82	0.15	1	-0.27
$\delta E_{15} + (1-\delta) E_{51}$	0.84	0.13	0.99	0.83
$\delta p_{15} + (1-\delta) p_{51}$	0.83	0.14	0.99	-0.25
$-1250 p_{55} \cdot p_{15} + 75.05$	-0.80	-0.13	-0.93	-0.72

4.2.8 Analysis of set-ups with double modes

Beforehand, there was an assumption that set-ups that contains two almost identical eigenfrequencies would behave differently from other set-ups. Figure 4.18 shows a range of

set-ups where the ones with double modes are marked with a star. As seen, there are set-ups with double modes that have both high and low VDV and therefore no conclusion can be drawn regarding them.

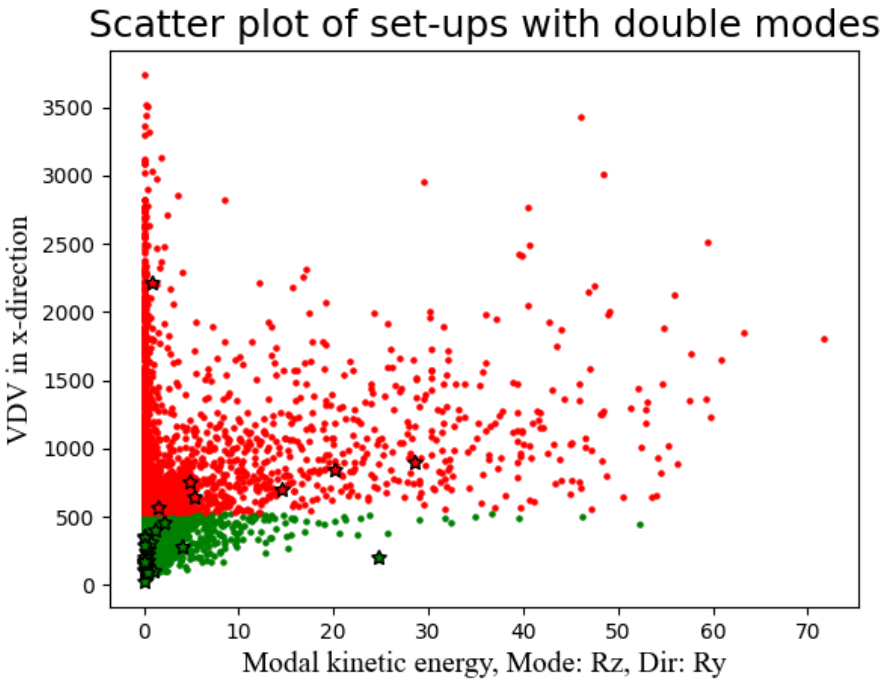

Figure 4.18: Scatter plot marking set-ups with double modes for the large DOE.

However, taking a further glance at a specific set-up with a double mode and make small deviations of the design parameters, the results in figure 4.19 are obtained. The graph shows the VDV in x-direction compared with E_{56}. The star marked set-ups with double modes are shown to deviate from the rest of the set-ups. To count as a double mode, the difference is put to be 0.3 rad/s in this case. The two modes close to each other are the Ry- and Rz-dominated, which may explain the high correlation with E_{56}. No conclusion regarding the performance can be stated, but the fact that the double modes have an interesting behaviour is clear from this result. Note that since the system is linear, the modes are independent, which is not the case in reality. No further investigation in the actual motion of the designs with double modes have been conducted, which may have changed the opinion regarding the conclusion.

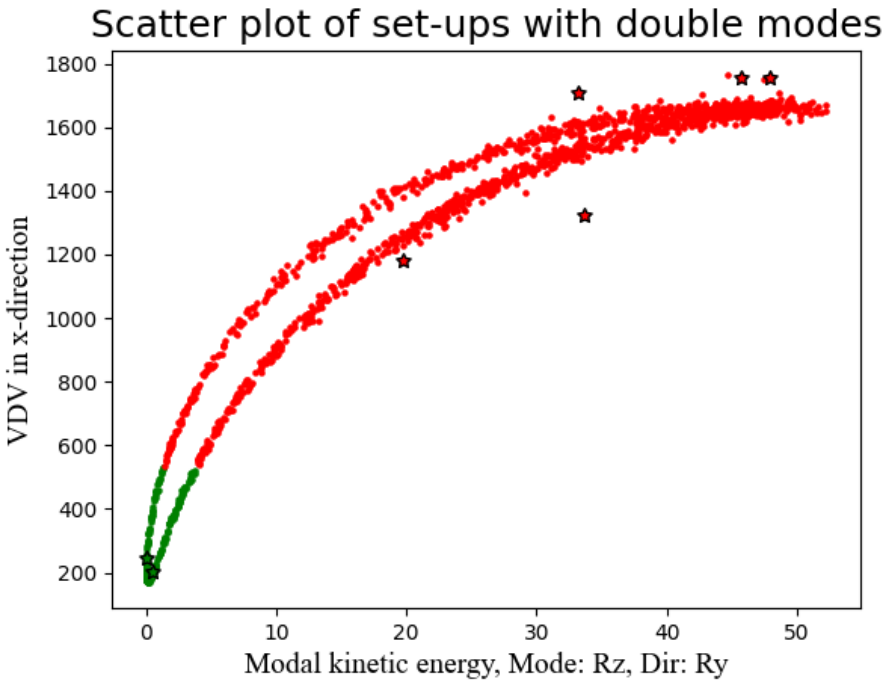

Figure 4.19: Scatter plot with low variations marking set-ups with double modes.

5

Discussion

The results that were presented in previous chapter will be discussed below. Focus will be on the reliability of the results and what sources of error that influences the final outcome. Further on, a comparison between earlier findings will be investigated as well as suggestions for future work.

5.1 Reliability of results

The results that have been obtained can be questioned in some senses. There are sources of error that needs to be discussed before drawing any conclusions. This includes a discussion of the reliability of the used methodology and the data that has been analysed.

5.1.1 The ordering of modes

One of the fundamental principles to find proper modal quantities for performance rating is the reordering of eigenmodes. Both the participation factors and modal kinetic energies relies on the reordering if a comparison should be applicable. But does every design have six distinct modes with a dominant direction for each DOF covered? In table 5.1 there is an example of a set-up that was generated from the complete LHS with 10 000 samples. This shows that there are two modes that are most dominant in y-direction and two modes in Rx-direction, while no mode is most dominant in z- or Rz-direction. This means for example that the modal quantity E_{33} would not have a physical meaning since no mode is dominant in z-direction which is a flaw in the methodology. Also, Mode 6 has a total modal kinetic energy of far above 100%, which is due to the mixed term that is not shown in the table but is explained in chapter 2.2.4. These terms are unphysical and are problematic when analysing the results.

Table 5.1: Example of a design were there is no dominant mode for every DOF.

	Mode 1	Mode 2	Mode 3	Mode 4	Mode 5	Mode 6
X-DOF	5.66	13.50	15.86	1.20	**63.77**	0.01
Y-DOF	2.41	**60.22**	**37.32**	0.04	0.01	0.00
Z-DOF	39.05	3.75	14.72	42.49	0.00	0.00
Rx-DOF	**39.14**	0.12	5.17	**55.36**	0.20	0.05
Ry-DOF	0.00	0.00	0.00	0.00	0.02	**105.98**
Rz-DOF	13.76	22.46	26.89	0.88	35.57	6.40
Eigenvalue [Hz]	14.17	15.38	15.45	17.51	23.47	81.29

As seen, it is not possible to organize the modes in a proper way for some designs, even with the naked eye. However, when doing a run with less variation on the input parameters this problem vanishes if the original design has clearly separated modes from the beginning. This means that the method may be bad when covering the whole spectra of possible designs, but it can be valid when analysing relatively well performing designs. Since VCC is mostly interested in the relatively good designs, the method can still be used if handled carefully.

5.1.2 The investigated parameter space

From the results, different DOEs provide different results. From all different simulations that have been conducted, the most suitable modal requirement has changed depending on what configuration that have been used as default. It is possible to see what quantities that have the highest potential to be a good requirement, but to specify a specific value is impossible with the simulations that have been made.

The best way to find a modal requirement would be to look at the complete LHS to see how all possible variations perform. However, it turned out to be harder than expected to cover the whole parameter space without making any too unphysical or unrealistic configurations. A method to easily remove poorly generated configurations would be beneficial for more proper results, but it is a fine line between having many realistic set-ups at the same time as the whole parameter space is covered.

5.1.3 Load dependency of reference value

Another thing that may question the reliability of the results is the fact that the reference value is load dependent. This means that the recommended modal quantity to use from this project is valid for this load condition, but not guaranteed to be accurate for other loads. VDV seems to be linear with respect to torque magnitude, but it is not sure that using the same methodology for other loading directions would provide the same results. However, this is the most commonly analysed load case for an engine set-up at VCC, and therefore the results can be used for dimensioning.

5.1.4 *Modal kinetic energy* vs. *Participation factors*?

As mentioned in section 2.2.4, the difference between modal kinetic energy and participation factor is not obvious. This means that for most of the simulations that have been done, the Spearman's correlation number between a specific modal kinetic energy parameter and VDV_x is almost the same as between the corresponding participation factor and VDV_x. So, which one should be used as a modal requirement of the performance?

The benefit with using participation factor is that the sum will always be 100 %, while for the modal kinetic energy, the mixed rotational terms E_{Rxy}, E_{Rxz} and E_{Ryz} need to be considered to make sure that the sum ends up at 100 %. This means that participation factors will provide a more understandable result. However, the modal kinetic energy is obtained immediately from Adams View while participation factors need to be postprocessed in order to be obtained. The postprocessing is not so easily done and it is not clear that someone will put that effort in the everyday use to evaluate the performance. In total, there are benefits of both these modal quantities and it is not obvious which one to use.

5.2 Recommendations for future work

During the work, some ideas on what to do next within this field have been born. This includes topics not covered in the scope of this thesis as well as thoughts that have appeared when analysing the results.

5.2.1 Deeper investigation for combination of quantities

Beforehand, one idea on how to find a modal quantity for performance evaluation was to try combinations off different modal properties as requirement. This was conducted and presented in chapter 4.2.7 and shows that the combined requirements perform well regarding correlation with VDV. However, the method to generate these plots was by manually trying combinations of modal properties and evaluate the outcome. The chosen quantities were only based on which ones that performed well alone. For further work, one suggestion would be to try artificial intelligence (AI) or machine learning algorithms to find an optimal combination of modal quantities. This would make it possible to try different relations, for example logarithmic functions, and not only sums and products. In conclusion, the idea that a combination of modal quantities would generate improved results is still valid, but the way to generate the combinations can be further developed.

5.2.2 Design of experiments

To improve future work even more, another suggestion would be to implement a *random seed* in each DOE, which makes it possible to reproduce the results if wanted, while keeping the DOE random. By using such seed, not only the results would be reproducible, also the debugging of the Python scripts would become easier.

Another thing to investigate would be how to find a way to discard any configurations that are not realistic or that provides unreliable results. One suggestion of that require-

ment could be to see if any number on the diagonal in the modal kinetic energy matrix is $< 50\%$, meaning that it is possible that another mode has a greater contribution in that direction. This would be beneficial when evaluating the complete parameter space.

5.2.3 Investigation of load dependency

One further suggestion for future work is to investigate the behaviour of different loading scenarios. This thesis only covers the investigation of a torque impulse around the y-axis, but different results would be obtained if other loading scenarios are investigated. This includes both torque impulses around other axes, force impulses as well as combination of them both. A bigger investigation of loading scenarios is necessary to get a full picture of the vibration isolation for a set-up in all possible conditions.

6
Conclusion

One of the main goal for this thesis was to find a modal requirement that could predict the time domain performance regarding vibration isolation. This turned out to be harder than expected and a specific value has not been obtained. However, the fundaments to find a requirement in the future are formulated and many ideas were born on the way. One thing that seems clear is that the old requirement of a certain percentage of modal kinetic energy for the x-mode in Ry-direction is not the most efficient to separate good and bad configurations. Probably, a combination of different modal properties is the most sufficient requirement to use, but the investigation of that does not fit the scope of this thesis.

When investigating deviations in parameter values, some conclusions can be made. First of all, the influence of the inertia matrix is present when evaluating the performance. This can be seen both when varying the size of the box as well as the orientation of the principal axes. Small changes in parameter values give a significant difference in VDV. Second of all, it can be seen that varying design parameters of a *bad* set-up leads to larger changes in VDV than doing the same variation for a *good* set-up. This shows that by having a well performing set-up as default, there is no need to worry about the tolerance of the design parameters.

A positive outcome of the thesis is the framework for model simulation. The framework allows the modeller to try different set-ups and find correlations between modal domain and time domain quantities. The ability to decide a combination of load cases provides the modeller with the opportunity to get a full evaluation of an engine set-up. It is also possible to compare other time domain data, not only VDV in x-direction which is the main quantity of interest for this work.

In conclusion, no modal requirement has been suggested to VCC but a base for investigating the problem further have been conducted. Small variations in design parameters may affect the performance significantly, but it depends on how well performing the engine set-up is at default. A recommendation for finding a sufficient modal requirement would be to further investigate how combinations of modal quantities can predict the vibration isolation. This can be implemented upon the already existing framework.

Bibliography

[1] "Eu ban on the sale of new petrol and diesel cars from 2035 explained," European Parliment. (Feb. 13, 2023), [Online]. Available: https://www.europarl.europa.eu/news/en/headlines/economy/20221019ST044572/eu-ban-on-sale-of-new-petrol-and-diesel-cars-from-2035-explained (visited on 04/24/2023).

[2] "Volvo cars to be fully electric by 2030," Volvo Cars Coporation. (Mar. 2, 2021), [Online]. Available: https://www.media.volvocars.com/global/en-gb/media/pressreleases/277409/volvo-cars-to-be-fully-electric-by-2030 (visited on 04/24/2023).

[3] F. Longoni, A. Hägglund, F. Ripamonti, and P. Pennacchi, "Powertrain modal analysis for defining the requirements for a vehicle drivability study," Nov. 26, 2022. [Online]. Available: https://doi.org/10.3390/machines10121120 (visited on 04/03/2023).

[4] B. Jacobson, *Vehicle Dynamics*. Department of Mechanics and Maritime Sciences, Chalmers University of Technology, 2019, ch. 1.

[5] Z.-F. Fu and J. He, *Modal Analysis*. Elsevier Science & Technology, 2001, ISBN: 9780080511788. [Online]. Available: https://search.ebscohost.com/login.aspx?direct=true&db=cat07472a&AN=clec.EBC298014&site=eds-live&scope=site&authtype=guest&custid=s3911979&groupid=main&profile=eds.

[6] R. R. Craig Jr. and A. J. Kurdila, *Fundamentals of structural dynamics*, 2nd ed. John Wiley & Sons, Inc., 1981, ISBN: 0-471-43044-7.

[7] E. H. Abed, D. Lindsay, and W. A. Hashlamoun. "On participation factors for linear systems." (Dec. 26, 1999), [Online]. Available: https://doi.org/10.1016/S0005-1098(00)00082-0 (visited on 03/16/2023).

[8] *Adams help*, Hexagon AB, Stockholm, Sweden, 2023.

[9] A. Boström, *Rigid body dynamics*, Course compendium, Chalmers University of Technology, 2018.

[10] J. Furlich, *Torque weighting vibration dose value to aid powertrain calibration process for transient torque maneuvers*. 2021. [Online]. Available: https://search.ebscohost.com/login.aspx?direct=true&db=edsstp&AN=edsstp.2021.01.1034&site=eds-live&scope=site&authtype=guest&custid=s3911979&groupid=main&profile=eds.

[11] M. Cieslak, S. Kanarachos, M. Blundell, C. Diels, M. Burnett, and A. Baxendale, "Accurate ride comfort estimation combining accelerometer measurements, anthropometric data and neural networks," *Neural Computing and Applications*, vol. 32, no. 12, pp. 8747–8762, 2020, ISSN: 0941-0643. [Online]. Available: http://dx.doi.org/10.1007/s00521-019-04351-1 (visited on 03/21/2023).

[12] P. Múčka, "Vibration dose value in passenger car and road roughness," *Journal of Transportation Engineering*, vol. 146, no. 4, 2020, ISSN: 2573-5438. DOI: 10.1061/JPEODX.0000200. [Online]. Available: https://ascelibrary.org/doi/abs/10.1061/JPEODX.0000200 (visited on 04/26/2023).

[13] M. Saraninezhad, M. Ramezani, and H. Falaghi, "Probabilistic assessment of wind turbine impact on distribution networks by using latin hypercube sampling method.," *2022 9th Iranian Conference on Renewable Energy & Distributed Generation (ICREDG), Renewable Energy & Distributed Generation (ICREDG), 2022 9th Iranian Conference on*, pp. 1–7, 2022, ISSN: 978-1-6654-0565-2. [Online]. Available: https://search.ebscohost.com/login.aspx?direct=true&db=edseee&AN=edseee.9804513&site=eds-live&scope=site&authtype=guest&custid=s3911979&groupid=main&profile=eds.

[14] M. D. McKay, R. J. Beckman, and W. J. Conover, "A comparison of three methods for selecting values of input variables in the analysis of output from a computer code," *Technometrics*, vol. 21, no. 2, pp. 239–245, 1979, ISSN: 00401706. [Online]. Available: http://www.jstor.org/stable/1268522 (visited on 03/16/2023).

[15] "Latin hypercube technique." (n.d.), [Online]. Available: https://abaqus.uclouvain.be/English/IhrComponentMap/ihr-c-Reference-LatinHypercube.htm#ihr-c-Reference-LatinHypercube (visited on 03/16/2023).

[16] G. W. Corder, *Nonparametric Statistics*. John Wiley & Sons, Incorporated, May 12, 2014, ch. 7.

[17] A. A. Shabana, "Reference kinematics," in *Dynamics of Multibody Systems*, 4th ed. Cambridge University Press, 2013, pp. 28–82. DOI: 10.1017/CBO9781107337213.003.

[18] B. H. Tongue and S. D. Sheppard, *Dynamics: analysis and design of systems in motion*. John Wiley & Sons, Inc., 2005, ISBN: 0-471-40198-6.

A

Input parameters for the models

In the tables below follows the input parameters used for the 3-DOF model and the 6-DOF model respectively.

Table A.1: All input data used to run the 3-DOF model.

Input variable	**Range**	**Unit**
r_1	[0.25, 0.30]	[m]
r_2	[0.3, 0.4]	[m]
m	[100, 140]	[kg]
k_1	[2.5e6, 3e6]	[N/m]
k_2	[2.5e6, 3e6]	[N/m]
k_3	[2.5e6, 3e6]	[N/m]
a	[0.1, 0.15]	[m]
b	[0.1, 0.2]	[m]
c	[0.1, 0.2]	[m]
γ	[0, $\pi/5$]	[rad]
F, Δt	[0, 0, 0], 0	[N], [s]
T, Δt	200e3, 7e-3	[Nm], [s]

Table A.2: All input data used to run the 6-DOF model.

Parameter	Value	Unit	Parameter	Value	Unit
Body			**Applied load**		
r_1	0.01	[m]	**F**	[0, 0, 0]	[N]
r_2	0.3	[m]	Δt	0	[s]
r_3	0.2	[m]	**T**	[0, 0.2e3, 0]	[Nm]
m	130	[kg]	Δt	0	[s]
rot_x	[-$\pi/30$, $\pi/30$]	[rad]			
rot_y	[-$\pi/30$, $\pi/30$]	[rad]			
rot_z	[-$\pi/30$, $\pi/30$]	[rad]			
Bushing 1			**Bushing 2**		
k_x	9e5	[N/m]	k_x	1e5	[N/m]
k_y	3e5	[N/m]	k_y	3e5	[N/m]
k_z	5e5	[N/m]	k_z	5e5	[N/m]
$k_{\psi\psi}$	0	[Nm/rad]	$k_{\psi\psi}$	0	[Nm/rad]
$k_{\theta\theta}$	0	[Nm/rad]	$k_{\theta\theta}$	0	[Nm/rad]
$k_{\varphi\varphi}$	0	[Nm/rad]	$k_{\varphi\varphi}$	0	[Nm/rad]
x	-0.3	[m]	x	-0.3	[m]
y	-0.3	[m]	y	0.3	[m]
z	-0.01	[m]	z	-0.01	[m]
Rx	$\pi/50$	[rad]	Ry	0	[rad]
Ry	$\pi/40$	[rad]	Ry	0	[rad]
Rz	$-\pi/60$	[rad]	Ry	0	[rad]
Bushing 3			**Bushing 4**		
k_x	9e5	[N/m]	k_x	9e5	[N/m]
k_y	3e5	[N/m]	k_y	3e5	[N/m]
k_z	5e5	[N/m]	k_z	5e5	[N/m]
$k_{\psi\psi}$	0	[Nm/rad]	$k_{\psi\psi}$	0	[Nm/rad]
$k_{\theta\theta}$	0	[Nm/rad]	$k_{\theta\theta}$	0	[Nm/rad]
$k_{\varphi\varphi}$	0	[Nm/rad]	$k_{\varphi\varphi}$	0	[Nm/rad]
x	0.3	[m]	x	0.3	[m]
y	-0.1	[m]	y	0.1	[m]
z	0.02	[m]	z	0.02	[m]
Rx	0	[rad]	Rx	0	[rad]
Ry	0	[rad]	Rx	0	[rad]
Rz	0	[rad]	Rx	0	[rad]

B

Spearman's correlation matrices

Here follows the Spearman's rank correlation matrices for time domain data vs modal domain data. The time data is divided into translational data and rotational data while the modal data is divided into stiffness and inertia, participation factors and modal kinetic energy. The data is from a run with 10 000 samples and a variation of the parameters of $\pm 50\%$.

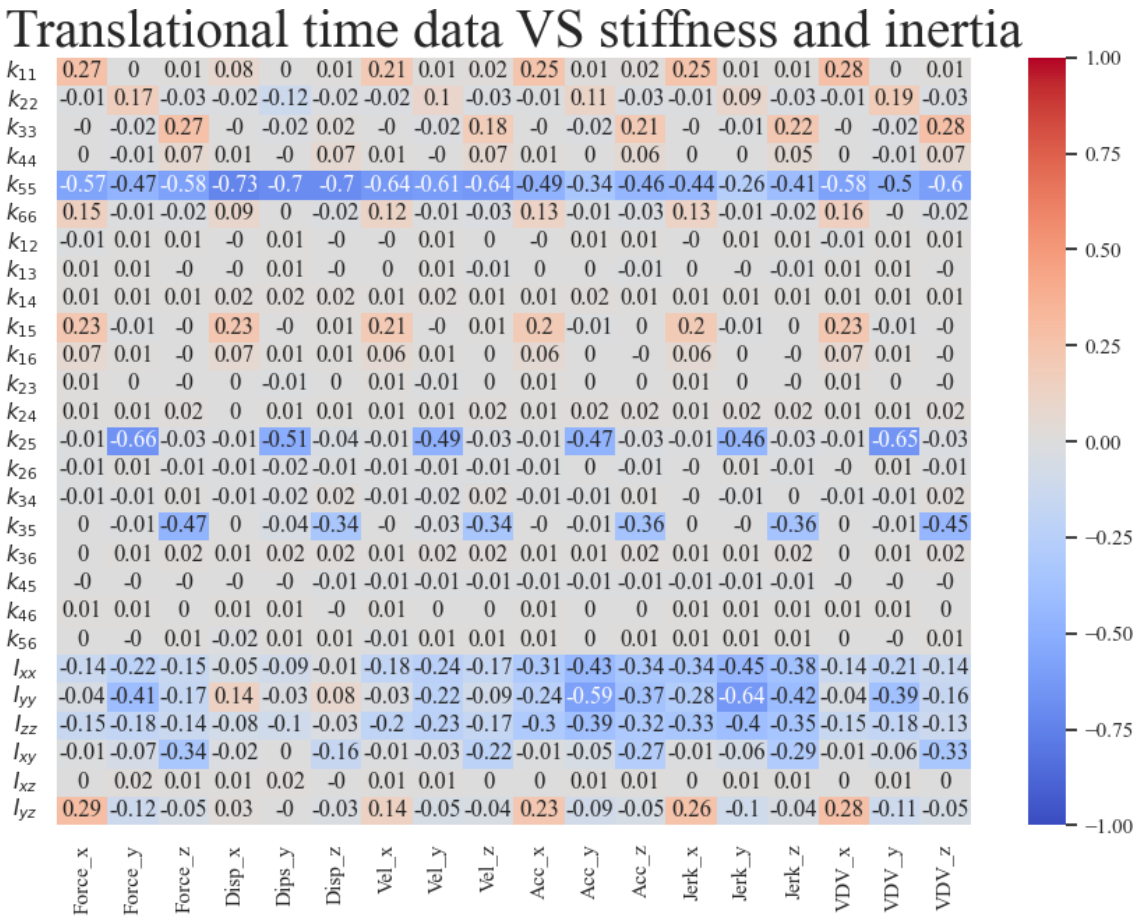

Figure B.1: Spearman's correlation between translational time data and stiffness and inertia.

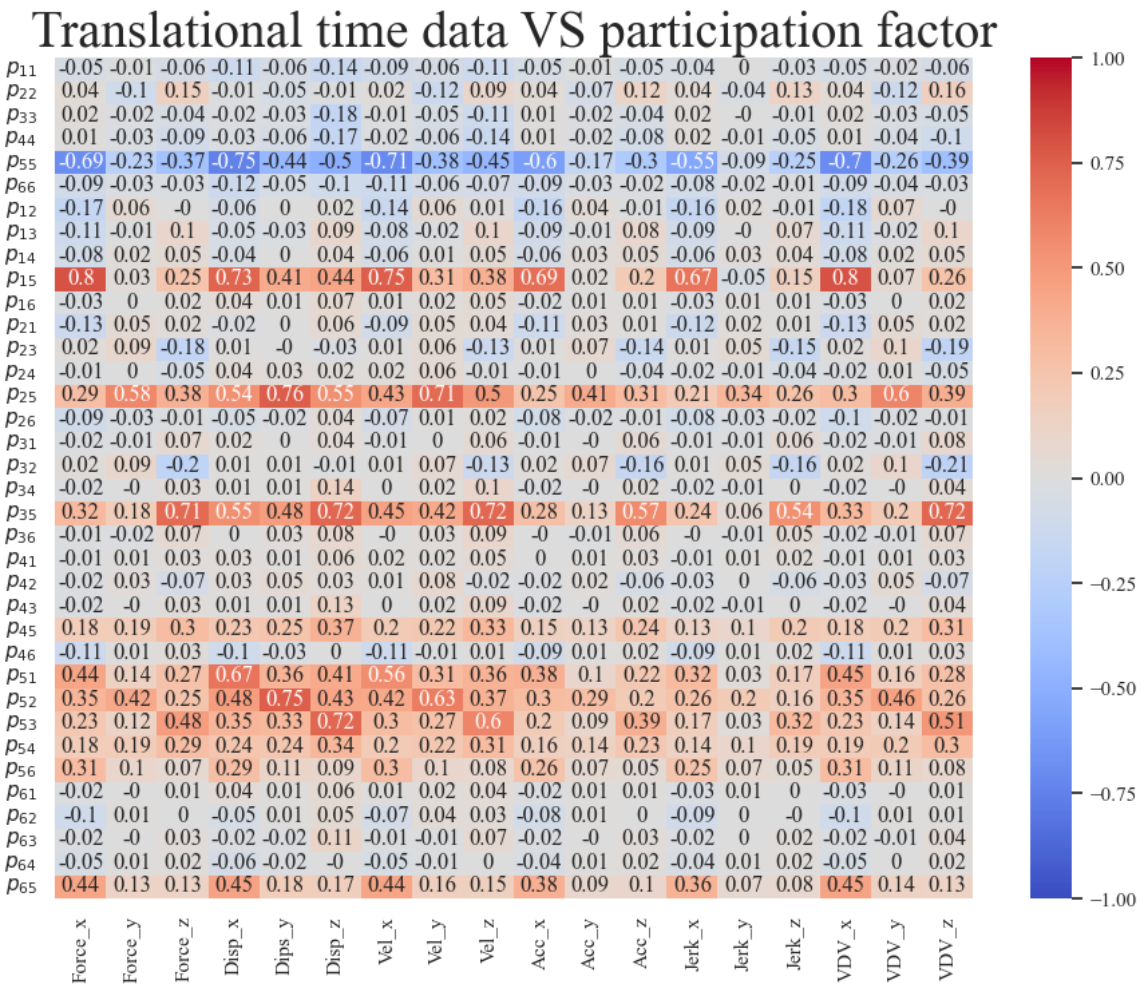

Figure B.2: Spearman's correlation between translational time data and participation factors.

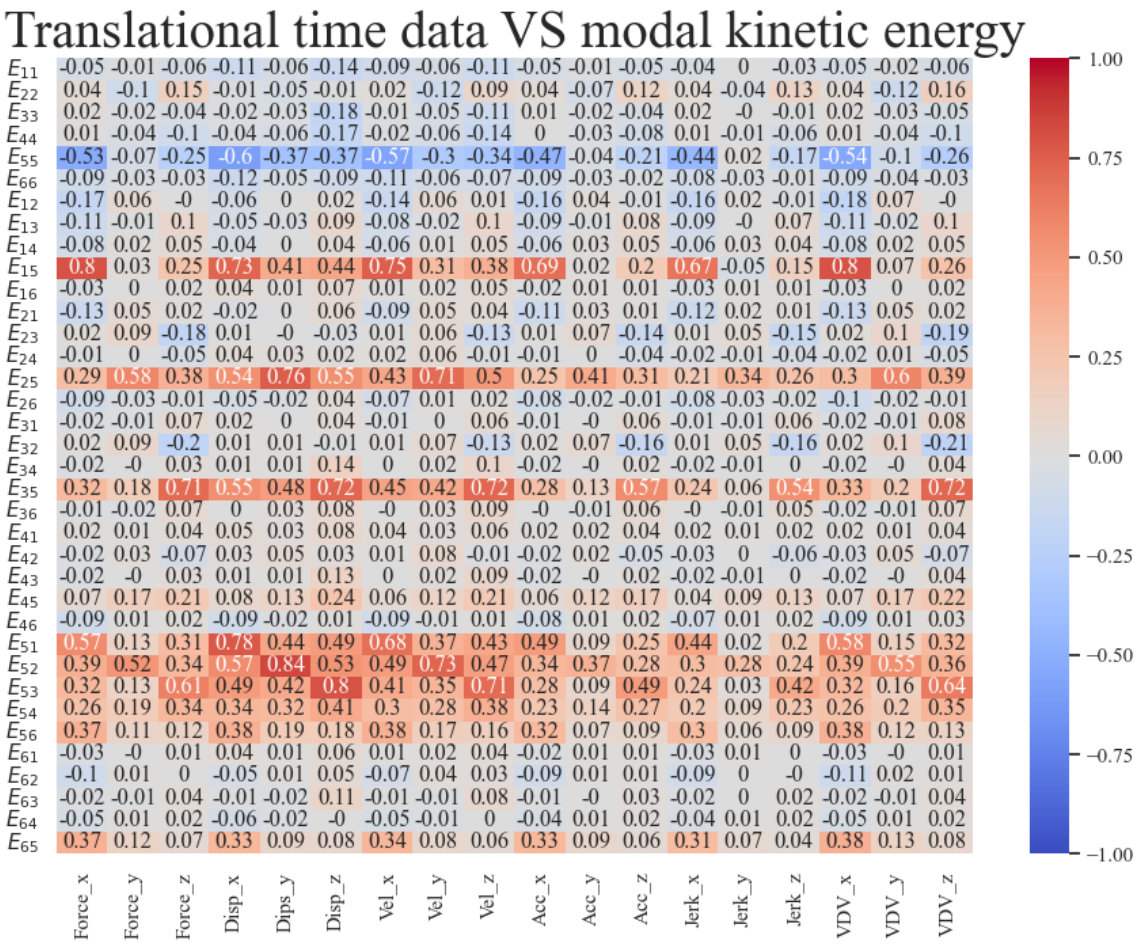

Figure B.3: Spearman's correlation between translational time data and modal kinetic energy.

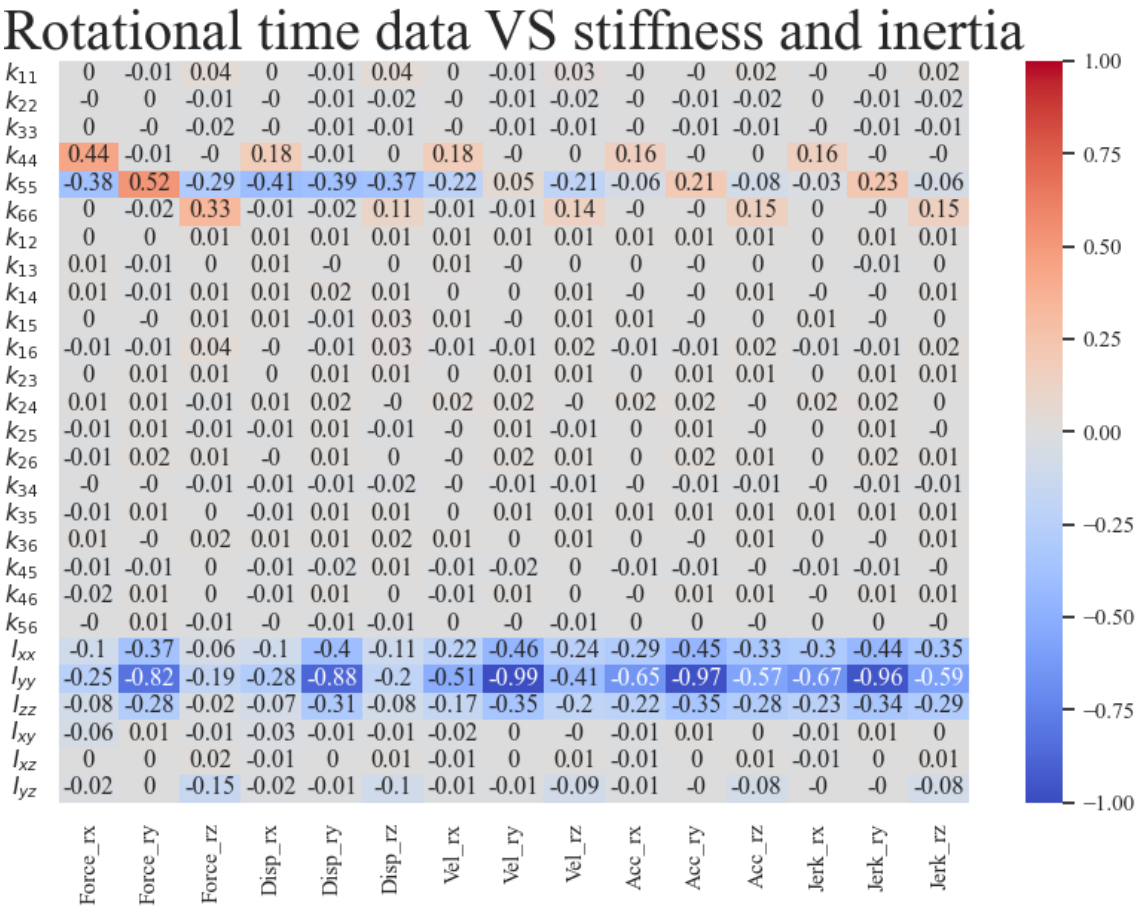

Figure B.4: Spearman's correlation between rotational time data and stiffness and inertia.

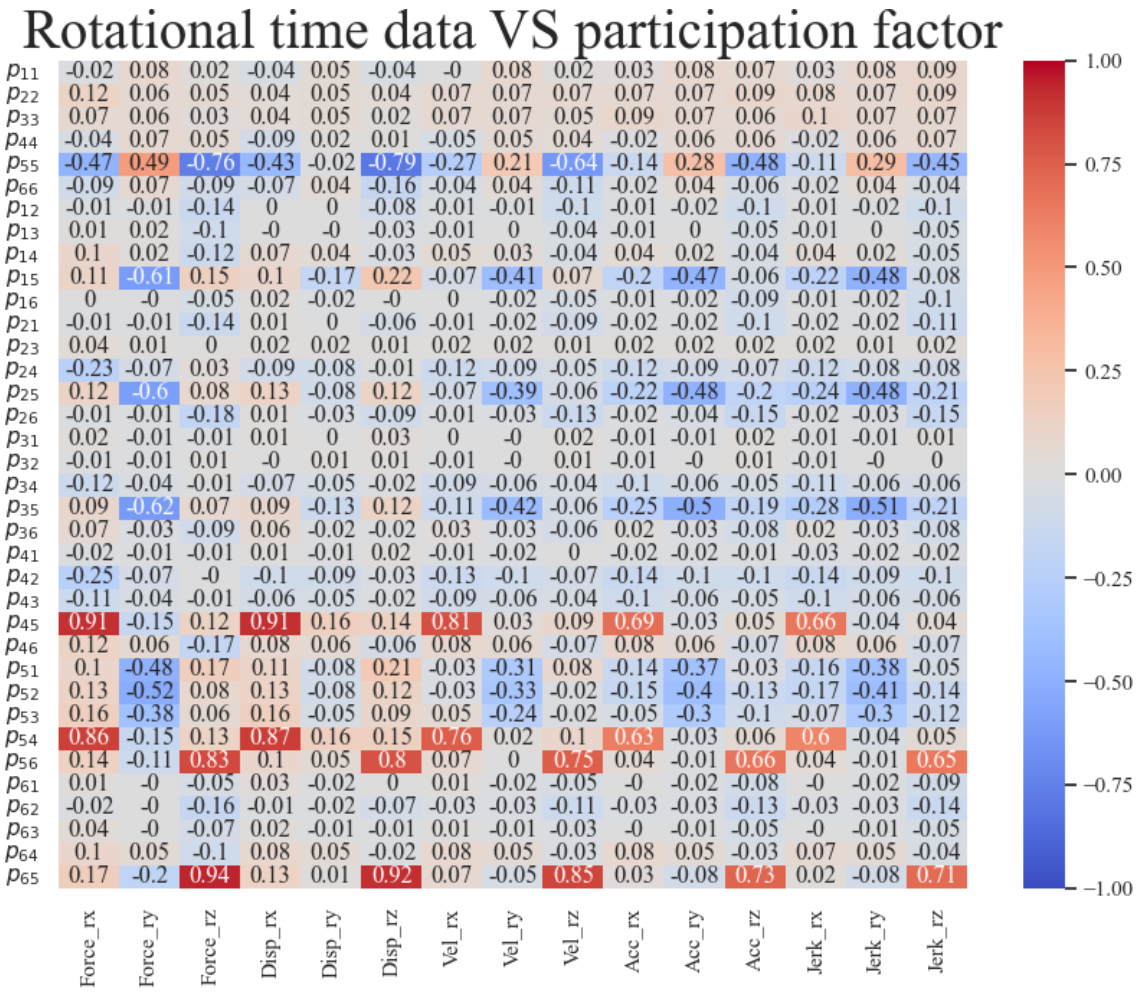

Figure B.5: Spearman's correlation between rotational time data and participation factors.

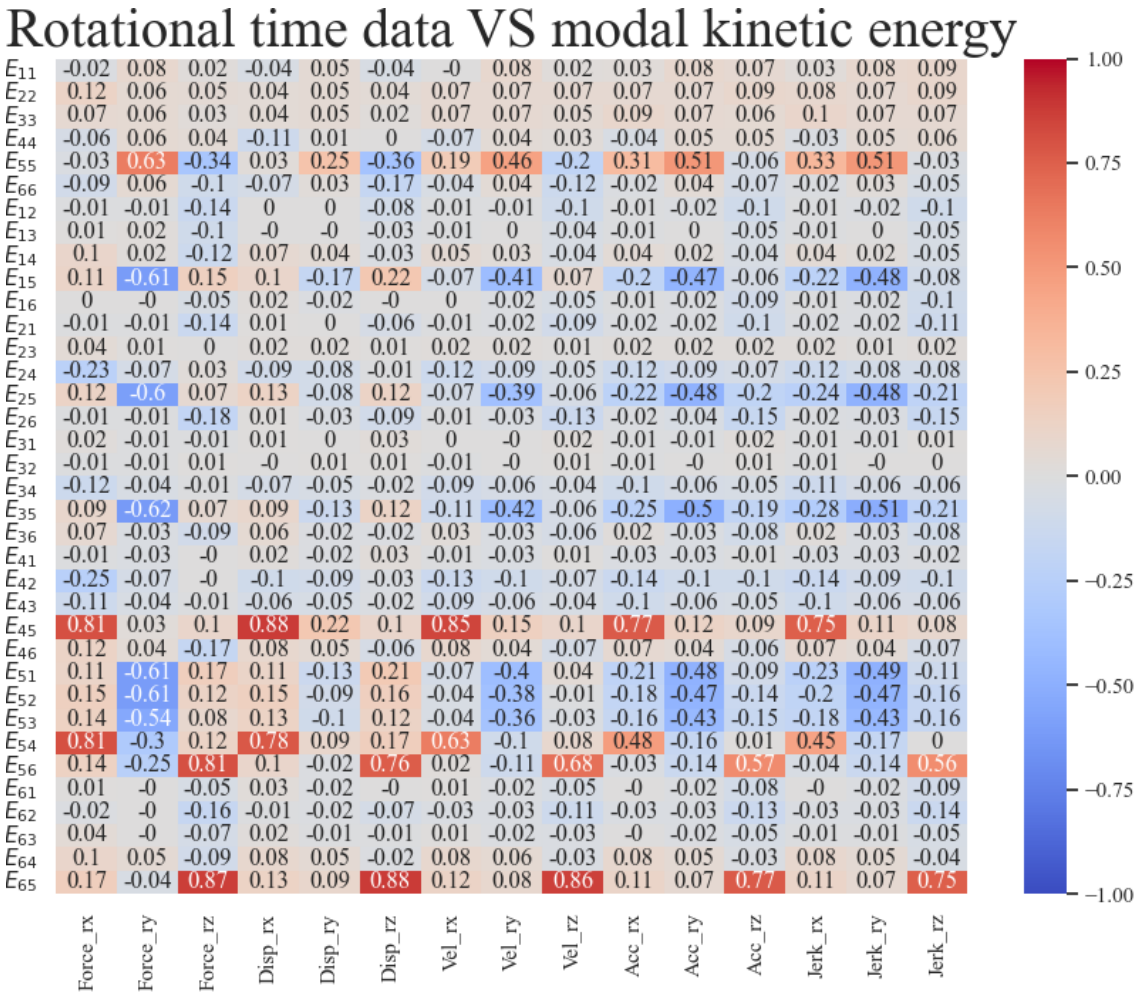

Figure B.6: Spearman's correlation between rotational time data and modal kinetic energy.

DEPARTMENT OF MECHANICS AND MARITIME SCIENCES
CHALMERS UNIVERSITY OF TECHNOLOGY
Gothenburg, Sweden
www.chalmers.se

CHALMERS
UNIVERSITY OF TECHNOLOGY